Wireless and Mobile Communication
Mekelweg 4, 2628 CD Delft,
The Netherlands

Antenna Beamforming for a 60 GHz Transceiver System

Muhammad Nasir Khan

August 31, 2009

MASTER OF SCIENCE THESIS

Student Number: 1391232

TU Delft

Faculty of Electrical Engineering, Mathematics and Computer Science Delft University of Technology

Antenna Beamforming for a 60 GHz Transceiver System

THESIS

Submitted in partial fulfillment of the requirement for the degree of

MASTER OF SCIENCE

in

ELECTRICAL ENGINEERING

by

Muhammad Nasir Khan
Born in Sialkot, Pakistan

COMMITTEE MEMBERS:

Professor	:	Prof. Dr. ir. Ignas Niemegeers (WMC-TU Delft)
Supervisor	:	Dr. ir. Gerard Janssen (WMC-TU Delft)
Mentor	:	Umar Hassan Rizvi (WMC-TU Delft)
External Examiner	:	Dr. ir. Geert Leus (Circuits and Systems)

Wireless and Mobile Communications (WMC)
Faculty of Electrical Engineering, Mathematics & Computer Science
Delft University of Technology

Abstract

The main target of a 60 GHz transceiver system is to obtain data rates close to gigabits per second (Gbps) over short distances. The 60 GHz band suffers from severe pathloss, inter-symbol interference (ISI) and a limited link budget. In order to improve the link budget, beamforming techniques are utilized. Antenna beamforming, i.e., combining signals from multiple receive antennas is one of the crucial aspects of the 60 GHz transceiver system. Adaptive antenna arrays are considered for the beamforming. A single carrier with frequency domain equalization (SC-FDE) is used for the modulation. In order to suppress the ISI, a cyclic prefix (CP) is used in SC-FDE. The effects of the physical parameters of antenna arrays on the RMS delay spread and BER have been investigated in LOS/NLOS condition. An algorithm for radio frequency (RF) level beamforming is proposed. The effects of perfect channel and non-perfect channel on the BER have been investigated using the proposed beamforming algorithm. The effects of the antenna array physical parameters on the BER using the proposed beamforming algorithm have also been investigated. It was seen that the BER improves after the implementation of the new beamforming algorithm. The 60 GHz band shows severe ISI which is improved by using the proposed beamforming algorithm.

Dedicated to my parents who have always
inspired and believed in me
May Allah Bless them!

Acknowledgement

This Master of Science (M.Sc) thesis was carried out at Technical University Delft (TU Delft), The Netherlands. It concluded a two year journey towards my degree in M.Sc. Electrical Engineering at the TU Delft. I would like to thank my supervisor dr.ir. G. J. M. Janssen and mentor Umar H. Rizvi, at the Electrical Engineering, Mathematics and Computer Science department of TU Delft. Their guidance and support have really been helpful. Without their advice this thesis would not have been the same. Dr.ir. G. J. M. Janssen is not only the best advisor that I have seen but also a role model as a researcher and a teacher to me. It was a big pleasure to be advised by him. Umar H. Rizvi was always there to help me whenever I was in trouble or whenever I didn't know what to do. He was always willing to help me and waited for me patiently until I found some results.

I feel kind of sorry that I cannot say more than 'thank you' to my parents. They supported me in every way and gave me a chance to study at TU Delft. I give my special thanks to my wife and son. I wish, I could say everyone's name here that helped me while I was staying at TU Delft. The reason why I cannot do that is that I needed help from so many people due to my lack of ability. I would like to thank my advisor, for introducing me to the project and for his guidance during classes and while doing my research. I have thoroughly enjoyed being a student of his and working under his guidance. I have learned a great deal and have expanded my spectrum of knowledge far beyond the 1's and 0's within a communication system.

My gratitude goes to all my lecturers for their knowledge and devotion which were the foundation of this work. I am also grateful to all my friends and colleagues, especially S.S. Gishkori, S. Aqeel, and D. Dony for their help and encouragement before and during this work. Last, but not least, I'd like to thank my family and friends who have supported me and encouraged me every step of the way. This study would not have been possible except for support through grants by the Higher Education Commission, Pakistan.

May God Bless You All!

Contents

Abbreviations

1-D	One dimensional
ADC	Analog to digital converter
AOA	Angle of Arrival
AF	Audio frequency
AWGN	Additive white Gaussian noise
B	Bandwidth
BER	Bit error rate
BF	Beamforming
BPSK	Binary phase shift keying
C	Channel capacity
CIR	Channel impulse response
CSI	Channel state information
CP	Cyclic prefix
DAC	Digital to analog converter
DFT	Discrete fourier transform
DOA	Direction of arrival
DDC	Digital down converter
dB	Decibel
ESPRIT	Estimation of signal parameters via rotational invariance techniques
FCC	Federal communication commission
FDE	Frequency domain equalization
FFT	Fast fourier transform
FIR	Finite Impulse response
FT	Fourier transform
GHz	Giga hertz
I/Q	In-phase / quadrature phase
IFFT	Inverse fast fourier transform
IDFT	Inverse discrete fourier transform
IBO	Input back-off

ISI	Inter-symbol interference
kHz	Kilo hertz
LOS	Line-of-sight
LMS	Least mean square
MUSIC	Multiple signal classification
MSE	Mean square error
MMSE	Minimum mean square error
NLOS	Non-line-of-sight
OFDM	Orthogonal frequency division multiplexing
PAPR	Peak to average power ratio
PDP	Power delay profile
PSAM	Pilot symbol assisted modulation
RMS	Root mean square
RDS	RMS delay spread
RLS	Recursive least square
RF	Radio frequency
R	Data rates
S	Signal power
SC	Single carrier
SNR	Signal to noise ratio
TDE	Time domain equalization
TOA	Time of arrival
ULA	Uniform linear array
UCA	Uniform circular array
UWB	Ultra wideband
WLAN	Wireless local area network

Variables

θ	Elevation Angle (in degree)
φ	Azimuth Angle (in degree)
Υ_{WBF}	BER after beamforming
Υ_{WOBF}	BER before beamforming
Δ	Distance between sub-Arrays
ζ	Elevation Angle in case of circular array (in degree)
α_m	Complex-valued amplitude
$\mathcal{F}$	Fast fourier transform
f_c	Center Frequency (in Hz)
r_0	Reference distance
ς_{WOBF}	RDS before beamforming
ς_{WBF}	RDS after beamforming
τ_{k_i}	Delay in signals within the array elements
τ_k	Propagation delay
K	Number of multipath
PL	Path loss
γ	Path loss exponent
M	Number of Antenna array elements
N	Noise Power
c	Speed of sound
$\bar{\tau}$	Mean delay
λ	Wavelength of signal
$N(t)$	AWGN noise vector
δ_N	Variance of the AWGN
$s(\theta)$	Transmitted signal
$a(\theta)$	Array steering vector
n	AWGN noise

$\mathcal{F}$	FFT
$\mathcal{F}^{-1}$	IFFT
P_t	Transmit power
P_r	Receive power
τ_{RMS}	RMS delay spread
$\delta(.)$	Delta dirac function
$h(t)$	Channel impulse response
σ^2	Noise variance
σ_τ	Standard deviation of the path delays
T_s	Sampling time
R	Radius of the UCA
$\delta^2_{n'}$	Input/output variance of linear system
$x(t)$	Baseband received signal
y	Beamformer output response
δ_{che}	Variance of the AWGN noise
θ_i	Scanning angle
θ_Δ	Scanning step size
$P_b(\mathcal{E}\|.)$	Conditional bit error probability
Q	Gaussian Q function

List of Figures

List of Tables

Chapter 1

Introduction

1.1 60 GHz Communication

It was the ever increasing demand for high data rates since the 1990s which has led to the invention of new technologies for high data rate communication systems. This enhanced the development of new devices which were light in weight, portable and cheap. Having all the advantages of these technologies, the inclination of bandwidth hungry people was greatly increased towards these technologies. In this way, the offices and the homes got rid of the cluttering of cables. Due to the high usage of bandwidth, the various available bands of 2.4 GHz and 5 GHz, rapidly started running out of spectrum. This high demand inspires the interest in exploring possibilities to use high frequencies with wide available bandwidths [2]. The 60 GHz band is one such example which has an abundance of licence free spectrum (5 GHz) available as shown in Figure 1.1. This shows the unlicensed frequency bands available for Japan, Europe and US along with their allowed transmit power. Communication systems that operate in this licence free band have the potential to achieve data rates of multiple gigabit per second. Therefore, 60 GHz is a viable candidate for short range communication with high data rates. According to Shanon's law,

$$C = B \log_2 \left(1 + \frac{P}{N}\right) \tag{1.1}$$

where C is the channel capacity, B is the channel bandwidth, P is the signal power and N is the noise power. In short, this principle states that with more available channel bandwidth and transmit power, higher data rates will be possible [3]. In Table 1.1, channel bandwidth, effective transmit signal power and the data rates R for different technologies have been compared. It shows

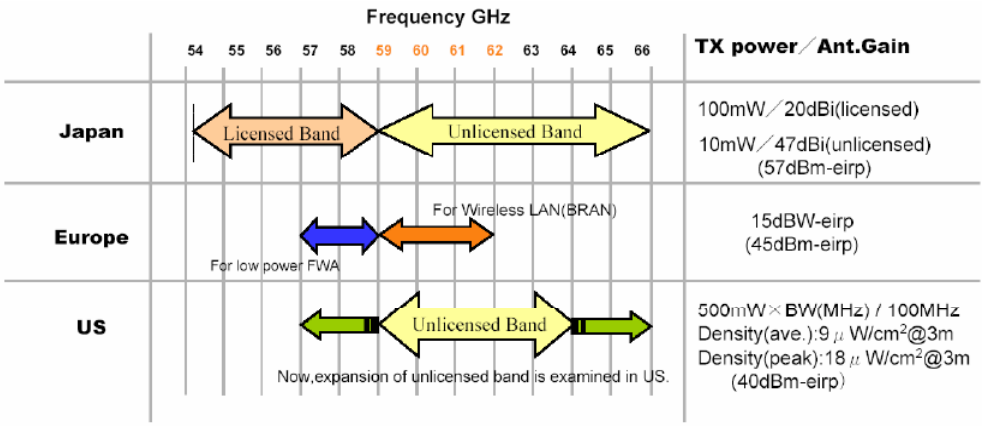

Figure 1.1: 60 GHz spectrum regulation [1].

the 60 GHz has more available data rate R in comparison to the IEEE 802.11n and ultra wideband (UWB).

	B	Effective P	Max. R
UWB	520 MHz	0.4 mW	80 Mbps
IEEE 802.11n	40 MHz	160 mW	1100 Mbps
60 GHz	2500 MHz	8000 mW	25000 Mbps

Table 1.1: Comparsion of 60 GHz with 802.11n and UWB [3].

1.1.1 Advantages of the 60 GHz band

There are numerous advantages of the 60 GHz band besides the high data rates as described below,

- **Licence free**, the major benefit of the 60 GHz is that it has an abundance of available licence free band of 5 GHz. It means that the operators do not need to buy the licence from the federal communication commission (FCC) in order to use this band. The licence buying process is very hectic and time taking.

- **Oxygen Absorption**, this feature of oxygen absorption makes 60 GHz more interesting in many applications. Due to the high oxygen absorption, the signal of 60 GHz greatly attenuates over distance. Therefore, the signal cannot travel far from the intended recipient [2]. Figure 1.2 shows the oxygen absorption of 60 GHz provided by FCC. This feature

of oxygen absorption enables higher frequency reuse at 60 GHz, as can be seen from Figure 1.3.

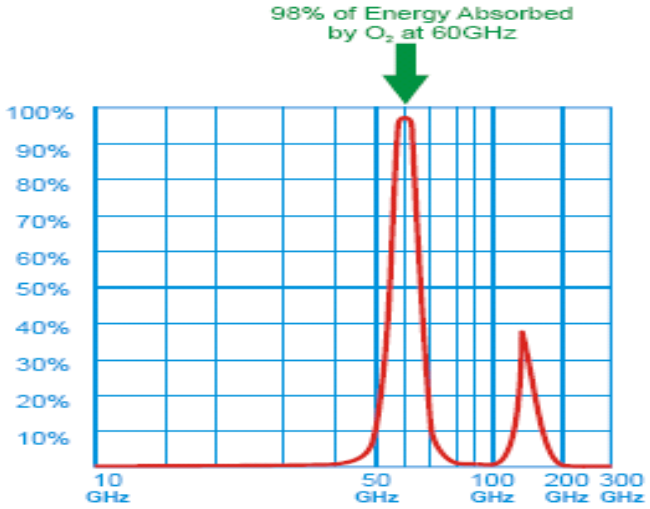

Figure 1.2: Oxygen absorption [2].

- **Antenna Directivity**, devices operating at high frequencies need highly directive or highly focused antennas in order to overcome the effects of the atmospheric absorption. Another benefit of the high frequency band is the fundamental relationship between the wavelength and the antenna size. Therefore, for 60 GHz highly focused with narrow beamwidth and small in size antennas can be fabricated. There is another important benefit of the narrow beamwidth, it makes the links highly immune to other interferers. Figure 1.4 shows the comparison of microwave antennas for 6 GHz and the antenna for the 60 GHz in terms of size and weight.

1.1.2 Challenges for 60 GHz

Along with the significant benefits, the 60 GHz band has many challenges to face with. Some of them are mentioned below.

- **Attenuation**, according to the Frii's transmission equation, the received power decreases with the square of the distance between the transmitter and the receiver. According to [4] , the channel measurements performed at various frequencies shows that the received power P_r is $P_r \propto d^{-n}$, where d denotes the separation of transmitter and receiver and n is an environment dependent factor commonly referred to

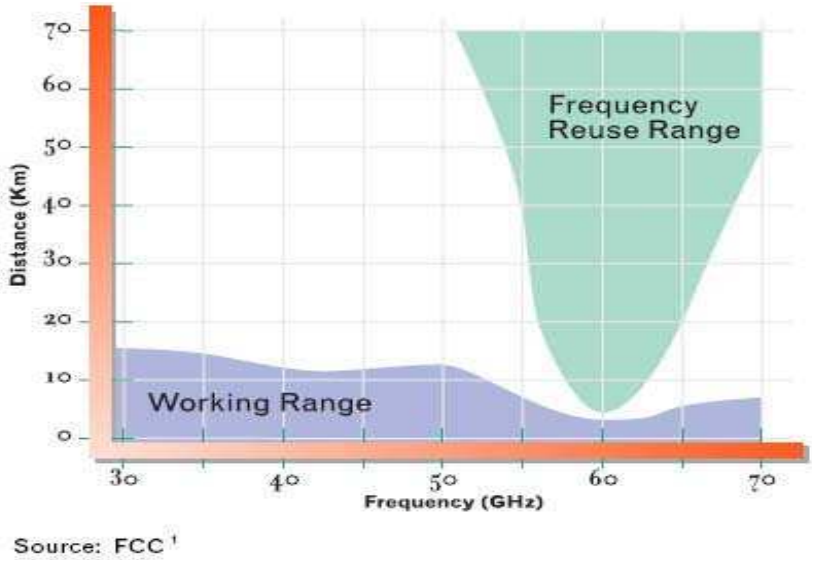

Figure 1.3: Frequency reuse [2].

Figure 1.4: Antennas for different bands [2].

as path loss exponent. The 60 GHz signal has a high path loss which affects the link budget.

- **Signal blockage**, another crucial problem of the 60 GHz is blockage of line-of-sight (LOS) signal due to the moving objects and/or the office furniture. It means that if the direct, i.e., LOS signal is blocked due to a moving objects or office furniture, then the receiver has to look towards the direction of arrival (DOA) of the strongest reflection, i.e., non-line-of-sight (NLOS) path.

- **Inter-symbol interference (ISI)**, it suffers from the ISI problem which is caused by multipath propagation. It degrades the bit error rate (BER) performance of the system

The possible solutions to the above mentioned problems, according to [5] are, transmit the signal with high gain antenna or use the adaptive phased array with the application of beamforming. In adaptive phased array, the phase and amplitude of each antenna element can be adjusted in real time. By using the antenna array, once the LOS signal is blocked, the array will be steered towards the direction of arrival of strongest reflection by the implementation of the beamforming technique. Beamforming algorithms, apart from having good performance, should have low complexity for real time implementation.

1.2 Previous Work

The crucial problem of 60 GHz is the blockage of the LOS signal due to moving objects and/or office furniture. Therefore, adaptive array utilization combined with the implementation of beamforming can be a possible solution. This solution has been utilized in variety of applications such as in seismic beamforming and in radar. Beamforming consists of DOA estimation and beam steering, with DOA estimation being the most critical step. Once the DOA has been estimated then the beam steering becomes straight forward. The problem of finding the DOA of a propagating waveform impinging on an array elements is a topic which has been studied since the beginning of 20th century [6]. Different classical adaptive beamforming algorithms, i.e., least mean square (LMS) and recursive least square (RLS) have been reported [6–8]. Today DOA estimation is still a popular research topic and there exist applications such as beamforming, localization and many more. In recent years, there has been plenty of research work on beamforming algorithms [7, 9, 10].

In general beamforming is an array processing approach used in combining the signals impinging on the antenna array elements. The beamformer is used to produce an array response with a high gain in the DOA of the strongest reflection. The basic principle of the beamforming approach is to coherently combine the received signals collected at the array elements, and then apply the adaptive algorithm in order to steer the signal power in a specific direction. Beamforming technique is very useful for short range communication systems. It is possible to use the beamforming in either of the transmitter side or the receiver side. It is used to reduce the transmission power, to increase the communication range and to cancel the interference. The applicability of beamforming has been found in numerous applications such as in radar, sonar, seismology, wireless communications, radio astronomy, speech and biomedicine.

Each of the above mentioned algorithms, i.e., LMS and RLS have their advantages and disadvantages based on the performance and implementation complexity. An efficient beamforming algorithm is the one which compensates for the hardware inaccuracies, does not add to complexity of the system significantly, converges fast and reduces the steady state error. There is a tradeoff between using these algorithms in terms of performance and implementation complexity. Beamforming is implemented using antenna arrays of arbitrary shape in order to achieve robustness and fast control of the beam. Widely studied antenna arrays are the uniform linear array (ULA) and the uniform circular array (UCA). The ULA can only provide DOA estimates with respect to the array axis (1D angle estimate). A circular array is needed if the estimation of both the azimuth and elevation angle is required [11]. Plenty of research has been done for the modulation of broadband wireless communication. Numerous techniques such as single carrier time domain equalization (SC-TDE), orthogonal frequency division multiplexing (OFDM) and single carrier frequency domain equalization (SC-FDE) have been reported in literature [12]. However, SC-FDE shows comparable performance to the OFDM and it has lower complexity than SC-TDE. It is also a power efficient scheme in terms of lower input-back-off (IBO) power requirements for power amplifier [12].

1.3 Problem Statement

The purpose of this thesis is to provide a beamforming solution in order to utilize the NLOS paths when the LOS path is blocked. We propose a low complexity (hardware wise) beamforming technique which is seen to be good for the 60 GHz transceiver systems. For the implementation of beamforming,

we investigate antenna arrays with linear and circular configurations. We utilize the SC-FDE scheme which is better in terms of power consumption. We utilize the proposed scheme of beamforming [13] in which the signal combing is done at the radio frequency (RF) level and then mixer and analog to digital converter (ADC) are used for further processing the signal. The advantages of using this scheme are that it is better in terms of additional hardware complexity and implementation cost for using one ADC and one mixer. For the conventional system, two ADCs and two mixers are required for each antenna element which enhance computational complexity and implementation cost of the system. The proposed technique is simple hardware wise, less expensive and power efficient as compared to the digital beamforming scheme.

The main contributions of this thesis can thus be outlined as follows:

- Investigates the impact of various antenna array parameters such as array elements M, inter-element spacing Δ of the ULA and the UCA on the RMS delay spread and the BER for 60 GHz. This gives us optimum values of inter-element spacing of the ULA and the radius of the UCA.

- Develops a beamforming scheme for 60 GHz transceiver system, and checks its performance in terms of BER by considering the ULA and UCA structures. Investigates the impacts of the Δ, M and array scanning step size on the BER improvement using the proposed beamforming scheme.

1.4 Report Outline

The rest of the thesis is organized as follow:

- **Chapter 2** presents two basic antenna array structures, i.e., linear and circular. In this chapter a simplified mathematical SC-FDE based signal model is presented. Then the channel model is presented along with the different important parameters such as power delay profile, time delay spread and the angular spread.

- **Chapter 3** outlines the antenna array considerations. It presents a mathematical derivation for BER calculation. It presents the comparison of BER analytically and by simulation. It provides simulation results which shows the impact of the physical parameters of the antenna array on the RMS delay spread and the average BER. It provides

the beamforming gains obtained using the investigated physical array parameters. It will then conclude with the results obtained by simulation showing the improvements in RMS delay spread and the average BER at 60 GHz.

- **Chapter 4** presents a new beamforming scheme for the 60 GHz transceiver system. It provides a motivation for the novel beamforming algorithm for 60 GHz. The performance of the scheme is presented and the impacts of various array parameters on its performance are investigated. It provides the beamforming gains obtained by the implementation of novel beamforming approach. It also outlines the effect of the array scanning step size. Then final conclusion of the proposed beamforming scheme for 60 GHz transceiver system will be presented.

- **Chapter 5** presents a final conclusion and future work.

Chapter 2

System Model

2.1 Introduction

LOS blockage is a crucial problem at 60 GHz. One feasible solution of this problem is the utilization for beamforming in order to steer the antenna array in the direction of arrival (DOA) of the strongest reflection. This chapter provides an overview of the array structure, a signal model and a channel model for the 60 GHz transceiver system. Two antenna array structures, i.e., an uniform linear array (ULA) and an uniform circular array (UCA) are defined in section 2.2. A generalized single carrier with frequency domain equalization (SC-FDE) based signal model for a 60 GHz transceiver system is presented in section 2.3. Then the channel model for the 60 GHz band will be explained along with various important propagation parameters in section 2.4. At last conclusions of the chapter are presented in section 2.5.

2.2 Antenna Arrays

An antenna array is a collection of antenna elements located at distinct spatial locations and are separated by certain distances. It has been reported in literature [14–16] that the preferred structures are the uniform linear array (ULA) and the uniform circular array (UCA). The linear antenna array geometry is simpler to implement than the circular one but the disadvantage is the symmetry (ambiguity) of the radiation pattern about the axis along the endfire[1], which is not the case in a circular geometry and also the circular geometry is more compact. Schematic representations of the ULA and the UCA are shown in the Figures 2.1 and 2.2 respectively.

[1] *endfire* is to be considered that direction which is parallel to that line which joins the antenna elements in a line

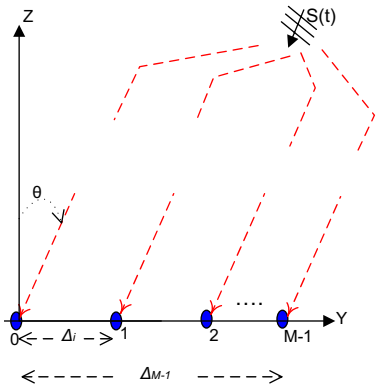

Figure 2.1: The uniform linear array.

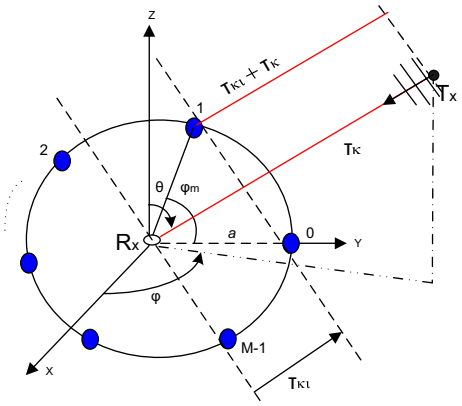

Figure 2.2: The uniform circular array.

The structure of the UCA allows the estimation for both the elevation angle θ down from z-axis and the azimuth angle φ measured counterclockwise from the x-axis. The origin of the coordinate is located in the center of the circle or in middle of the ULA. For the UCA and the ULA, the delays for the m-th antenna array element with respect to center for the UCA and with respect to the first antenna array element for the ULA are given by the equations (2.1) and (2.2) respectively [14],

$$\tau_m = \left(\frac{a}{c}\right)\left(\sin\left(\theta\right)\cos\left(\varphi - \varphi_m\right)\right), \tag{2.1}$$

$$\tau_m = \left(m-1\right)\left(\frac{\Delta}{c}\right)\left(\sin\left(\theta\right)\right), \tag{2.2}$$

where a is the radius of the UCA, $\varphi_m = \frac{2\pi m}{M}$, M is the number of array elements and $m = 0, 1, ..., M-1$, θ is the elevation angle and φ is the azimuth angle, Δ is the inter-element spacing of the ULA, c is the speed of light and τ_{m_k} represents the relative delay introduced at the array elements with respect to the center for the UCA and the delay with respect to the first element for the ULA.

2.3 Signal Model

In order to select a modulation scheme for 60 GHz, a number of parameters such as characteristics of the propagation channel, use of high gain antenna array and the RF impairments need to be considered [17]. Different schemes such as orthogonal frequency division multiplexing (OFDM), SC-TDE and SC-FDE have been reported in [12]. In a traditional SC-TDE, equalization was done in time domain. Therefore, with the time domain equalization, the scheme becomes computationally intensive and also complex for a channel with severe inter-symbol interference (ISI). This complexity of the SC-TDE has been overcome by introducing the frequency domain equalization (FDE) [12]. In the SC-FDE scheme, the data is transmitted block wise in the time domain and then the equalization is performed in the frequency domain. SC-FDE has comparable complexity to OFDM but it has lower peak to average power ratio (PAPR). This scheme, due to the lower PAPR, has the advantage of lower input back-off (IBO) requirement for the power amplifier and requires lower ADC dynamic range which makes the SC-FDE, a low cost and power efficient alternative to OFDM. To combat the crucial problems

of broadband wireless communication, such as ISI, a cyclic prefix is used in SC-FDE [12]. A detailed description of SC-FDE can be found in [12, 18]. A simplified block diagram of the SC-FDE scheme with antenna array is shown in Figure 2.3.

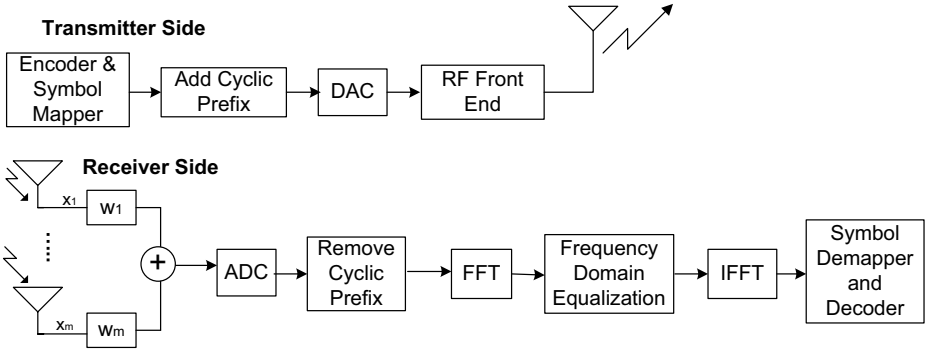

Figure 2.3: SC system model.

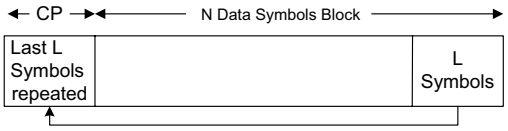

Figure 2.4: Cyclic prefix block.

From the transmitter side, the mapped data symbol vector $\mathbf{s}$ is transmitted by adding a cyclic prefix (CP) in front of each block. A cyclic prefix with length L symbol is formed by reproducing the sequence of the last L transmitted symbols and adding these symbols to the beginning of the block before transmission as shown in the Figure 2.4. The signal is then converted into its analog form using a digital-to-analog converter (DAC) to make the signal suitable for transmission, and then the signal is transmitted from the RF front end.

At the receiver, by assuming an ideal front end, the received signal vector after antenna beamforming is given as,

$$y^c(t) = [s^c(t) * h(t,\theta)]\, a(\theta) + n^c(t)\, a(\theta), \tag{2.3}$$

where y is the received array output, s represents the transmitted signal, h represents the channel impulse response, $*$ represents the convolution operation, n is the additive white Gaussian noise (AWGN), c is the cyclic prefix

superscript and $a(\theta)$ is the array response of the antenna array. The array steering vector for the ULA and the UCA for equally spaced elements M is given by the equations (4.1) and (4.2) [19];

$$a(\theta) = \sum_{m=1}^{M} e^{j\left(\frac{2\pi m\Delta}{\lambda}(\sin(\theta))\right)} \tag{2.4}$$

$$a(\theta, \varphi) = \sum_{m=1}^{M} e^{j(\zeta_0 \cos(\varphi_0 - \varphi_m) - \zeta \cos(\varphi - \varphi_m))} \tag{2.5}$$

where $\zeta = \frac{wa}{c}(\sin(\theta))$, w/c is the wave number, a is the radius of the UCA array and φ_m is the spatial location of the respective array element. In case of the ULA, Δ is the distance between the array element also known as inter-element spacing and is supposed to be less than $\lambda/2$, λ is the wavelength of the signal and θ is the angle of arrival (AOA) of multipath.

Since the convolution is the linear multiplication function, we can re-write the equation (2.3) as,

$$y^c(t) = s^c(t) * h(t, \theta).a(\theta) + n^c(t).a(\theta), \tag{2.6}$$

Let $\widetilde{h}(t) = h(t, \theta).a(\theta)$ and $\widetilde{n}(t) = n^c(t).a(\theta)$, then equation (2.6) can be written as,

$$y^c(t) = s^c(t) * \widetilde{h}(t) + \widetilde{n}(t), \tag{2.7}$$

By the removal of the CP after the ADC block, the above equation (2.7) can be written as,

$$y = s \otimes \widetilde{h} + \widetilde{n}, \tag{2.8}$$

After applying the fast fourier transform (FFT), the vector at the output of FFT block can be represented by the following equation,

$$Y_m = \mathcal{F}_m\left(\widetilde{h}\right)\mathcal{F}_m(s) + \mathcal{F}_m(\widetilde{n}), \tag{2.9}$$

where $\mathcal{F}_m$ represents the m-th sample of the FFT. Assuming perfect channel state information (CSI) at the receiver, the frequency domain equalization (FDE) can be applied at the output from FFT block to invert the effect of channel. The FDE is a point wise division of the FFT output by the estimated channel transfer function. Then the resulting equation can be represented as,

$$\hat{Y}_m = Y_m / \mathcal{F}_m\left(\widetilde{h}\right) = \mathcal{F}_m\left(s\right) + \frac{\mathcal{F}_m\left(\widetilde{n}\right)}{\mathcal{F}_m\left(\widetilde{h}\right)}, \tag{2.10}$$

Now by taking the inverse FFT (IFFT) of the above equation (2.10), we get the resulting estimated symbol $\hat{s}$ as,

$$\hat{s}_m = s_m + \mathcal{F}_m^{-1}\left(N_t\right), \tag{2.11}$$

where $N_t = \left(\mathcal{F}_0\left(\widetilde{n}\right)/\mathcal{F}_0\left(h\right), \cdots, \mathcal{F}_{N-1}\left(\widetilde{n}\right)/\mathcal{F}_{N-1}\left(h\right)\right)$. The output estimated data vector is then passed to the demapper and decoder.

2.4 Channel Model

The channel parameters deal with the fidelity of the received signal. It is important to estimate the characteristics of the medium through which RF waves propagate. Path loss, time delay spread and angular spread are the crucial parameters of the radio channel. Path loss is important in calculating the link budget of the RF system. The channel impulse response for the 60 GHz channel model is given by the following equation [20],

$$h\left(\tau, \theta_{rx}\right) = \sum_j A^j C^j\left(t - \tau^j, \theta_{rx} - \Theta_{rx}^j\right) \tag{2.12}$$

$$C^j\left(t, \theta_{rx}\right) = \sum_k \alpha^{(j,k)} \delta\left(t - \tau^{(j,k)}\right) \delta\left(\theta_{rx} - \Theta_{rx}^{(j,k)}\right) \tag{2.13}$$

where,
h represents the channel impulse response,
t represents the time index,
θ_{rx} represents the elevation angle at the receiver,
A^j denotes the gain for the j-th cluster,
C^j denotes the j-th cluster,
$\delta(.)$ represents the Dirac delta function,
$\tau^{(j,k)}$ and $\Theta_{rx}^{(j,k)}$ represent the time delay and angular coordinates of the k-th multipath of the j-th cluster,
$\alpha^{(j,k)}$ denotes the amplitude of the k-th multipath of the j-th cluster.

The received signal consists of clusters including the LOS and NLOS multipath signals with the first order reflection and second order reflections

due to the ceiling, walls and/or floor [20]. In equation (2.12), the clustering approach has been adopted, where each cluster consist of several rays which are spatially separated in time and angular domain. Since in real scenarios, these clustering parameters, i.e., time delays and the angular spread are the time varying functions because of a non-stationary environment. However, the rate of variations in these parameters will be relatively slow due to limited movement. It has been observed in [20], that for the 60 GHz channel, the main propagation path includes the LOS, first order reflections and second order reflections. The channel impulse response for 60 GHz has been plotted for the time of arrival (TOA) and the elevation angle θ in LOS and NLOS scenarios as can be seen from the Figures 2.5 and 2.6 respectively.

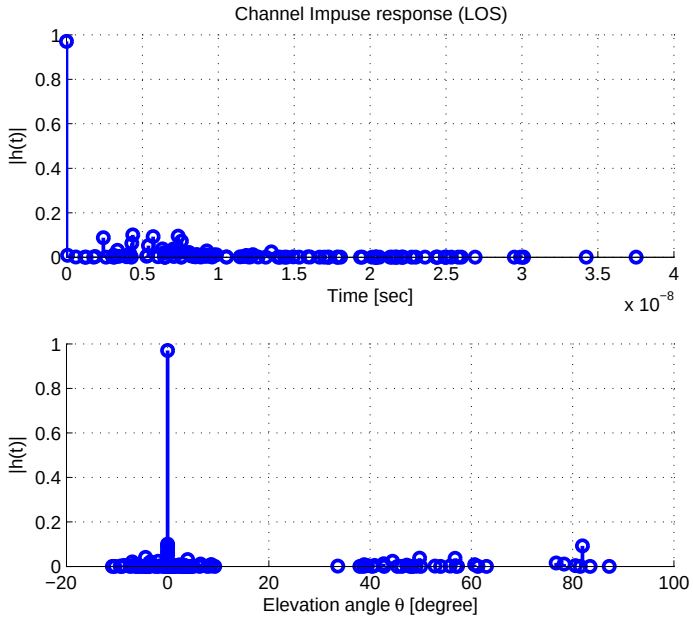

Figure 2.5: Channel impulse response for LOS.

The path loss has been reported to be about 30dB higher than at 2 GHz in free space for a fixed separation between transmitter and receiver [5]. Apart from free space path loss, signals in this frequency band face severe attenuation while passing through walls and floor partitions. A number of studies [5, 21] have been carried out in modeling of the 60 GHz channel. These studies indicate that path loss increases with frequency. Furthermore, human activity inside the buildings has a direct effect on the propagation of the signals. Though most of the times, transmitter and receiver are stationary but human activity can cause temporal fading and the effects of fading

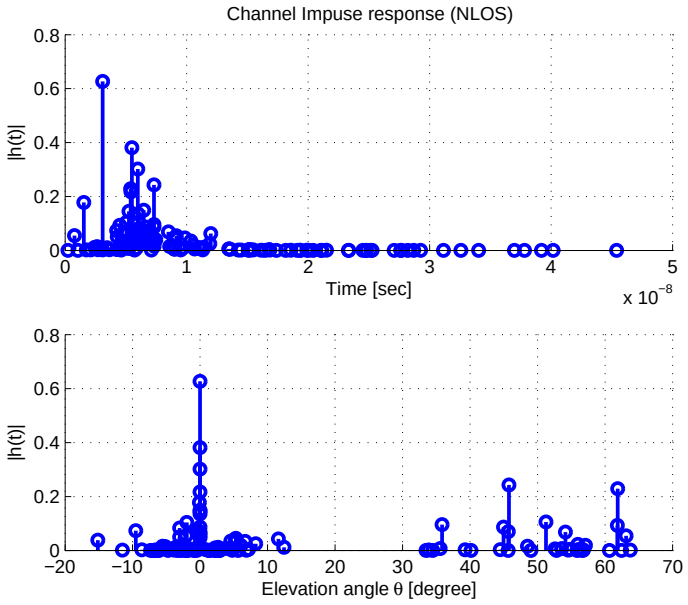

Figure 2.6: Channel impulse response for NLOS.

depends on the speed and amount of activity.

Since the bandwidth is quite large, so the propagation channel can cause frequency selective effect on the signal. This frequency selective effect produces the ISI in the signals. According to [5], multipath can be greatly suppressed by using directional transmit and receive antennas which results in a quite smooth frequency responses. It is also reported in [5] that the adaptive beamformer is a good candidate to greatly reduce frequency selectivity caused by multipath. Since for the beamformer, the beam is steered towards the direction of arrival of the strongest reflection electronically. Moreover, the effects of multipath can vary with the dimensions of propagation space and more importantly with the location and concentration of room furniture. These effects are reflected in the power delay profiles. It has been reported in [4] that the RMS delay spread can drastically affect the efficiency of the system if it is larger than the duration of a symbol. The description of the various characteristics of the channel model which affect the received signal are presented in the following subsections.

2.4.1 Path Loss

This parameter describes the overall decrease in the field strength with the increasing distance between the transmitter and the receiver. The path loss

can be defined by the following equation [22],

$$PL = 10 \log \left(\frac{P_t}{P_r} \right) \tag{2.14}$$

where P_t is the transmitted signal power and P_r is the received signal power and PL represents the path loss in decibel (dB). The path loss at distance r from the transmitter can be calculated by the following equation [22],

$$PL\,(r) = PL\,(r_0) + 10 \times \gamma \log \left(\frac{r}{r_0} \right) \tag{2.15}$$

where the $PL\,(r_0)$ denotes the free space path loss at some reference distance r_0, γ represents the path loss exponent and its value depends on the propagation environment. The path loss exponent for a 60 GHz system for LOS and NLOS in case of office and home environment have been observed in [23, 24] for different scenarios. It is seen from [25] that the path loss exponent for indoor environment is to be considered mostly $\gamma = 2$ or less than 2 for LOS scenarios and for the NLOS scenarios it is to be considered $\gamma = 3.5 - 4$. It has been reported in [8, 22] that the path loss increases with the increment of frequency due to absorption. Therefore, for the 60 GHz band there will be significant path loss which results in a decreased link budget.

2.4.2 Power Delay Profile (PDP)

The received signals from the channel are attenuated in amplitude, delayed in time and shifted in phase [26]. This type of channel has been modeled in equation (2.12). The multipath spread of the transmitted signal due to delayed reflections is usually known as the time dispersion of the transmitted signal. The degree of time dispersion of the signal can be measured by power delay profile (PDP). This time dispersive nature indicates the distribution of the transmitted power over different reflections in a multipath environment. The PDP can be calculated by using the following equation [8, 26],

$$p\,(\tau) = E\left[\left| h\,(t, \theta_{rx}) \right|^2 \right] \tag{2.16}$$

Figures 2.7 and 2.8 show the channel response and PDP for 60 GHz channel in LOS scenario respectively. Figures 2.9 and 2.10 show the channel response and PDP for 60 GHz channel in NLOS scenario respectively. The other important parameter of the 60 GHz channel model is the time delay spread which is described in the next subsection.

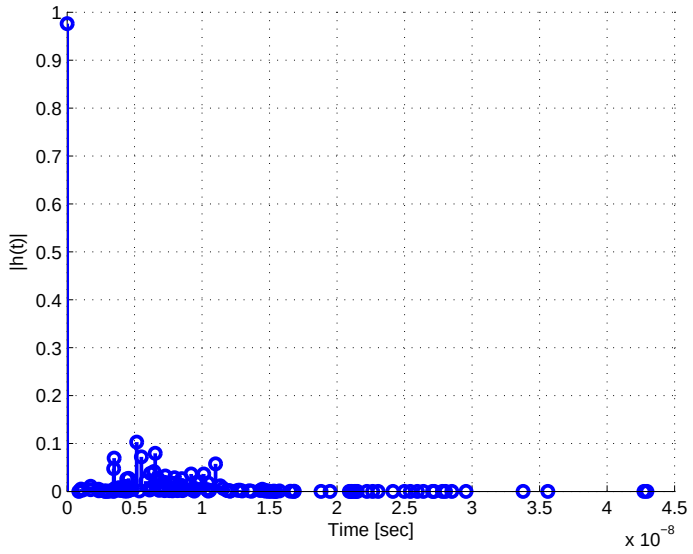

Figure 2.7: Channel realization in LOS case.

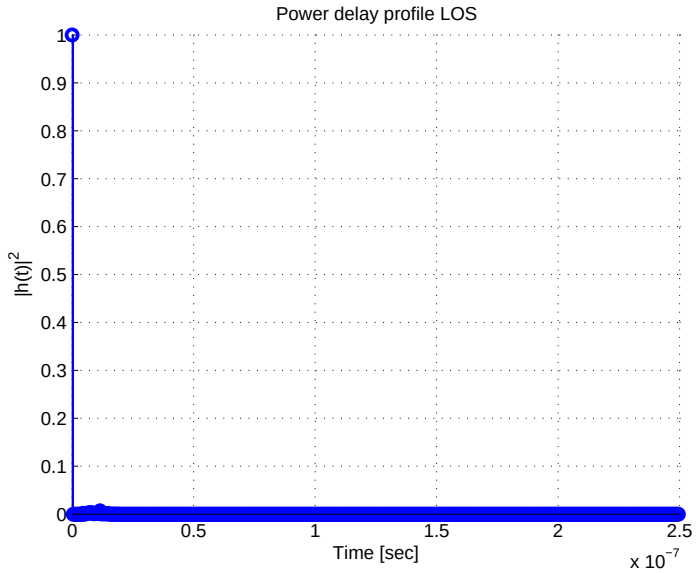

Figure 2.8: Power delay profile in LOS case.

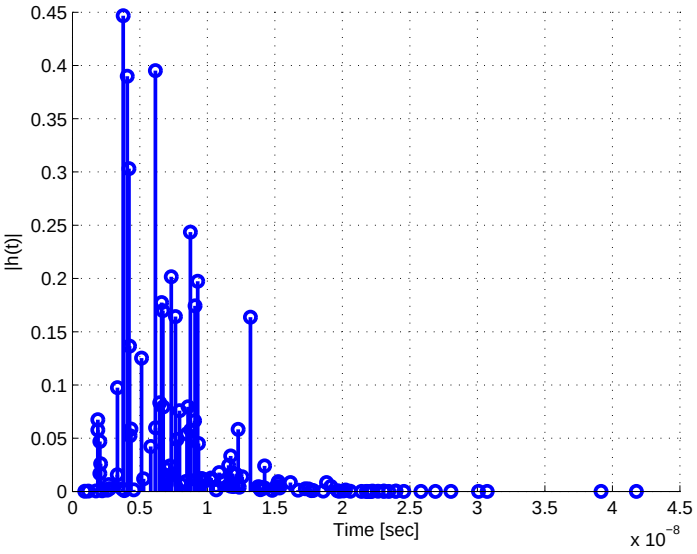

Figure 2.9: Channel realization in NLOS case.

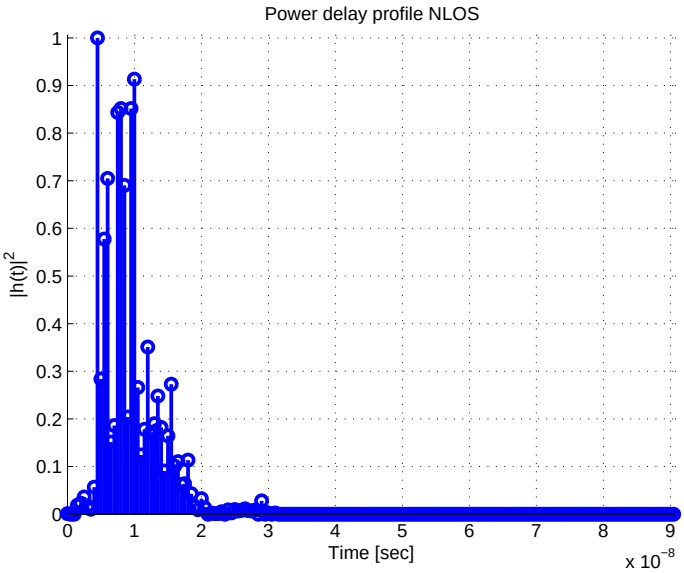

Figure 2.10: Power delay profile in NLOS case.

2.4.3 Time Delay Spread

It has been mentioned already that the transmitted signal reaches the receiver either through LOS or NLOS (multipath) propagation. The NLOS signal varies widely in terms of power and or time dispersion in the RF channel which is caused by multipath. There is an important parameter τ_{RMS}, i.e., RMS delay spread which is a good measure of the multipath power spread in the RF propagation channel. It is the square root of the 2nd moment of the power delay profile and it gives an indication of the nature of ISI [26]. In [26], it has been defined that the RMS delay spread is the standard deviation of the path delays in the power delay profile and is given by the following equation,

$$\sigma_\tau = \sqrt{\frac{\sum_k (\tau_k - \bar{\tau})^2 P(\tau_k)}{P(\tau_k)}} = \sqrt{\overline{\tau^2} - (\bar{\tau})^2}, \tag{2.17}$$

where,

$$\bar{\tau} = \frac{\sum_k \alpha_k^2 \tau_k}{\sum_k \alpha_k^2}, \tag{2.18}$$

where τ_k is the time delay, α_k is the amplitude, $P(\tau_k)$ is the signal power of path k and $\bar{\tau}$ is the mean delay value in the power delay profile. It is seen that a signal with symbol period T_s will experience ISI if its symbol period is much less than τ_{RMS}, i.e., $T_s \ll \tau_{RMS}$ and it will experience insignificant ISI if $T_s \gg \tau_{RMS}$. The ISI is a major problem in high speed wireless communication networks. It has been reported in [4] that by using the symbol period $T_s > 10\tau_{RMS}$ is good enough to limit the effect of ISI. Therefore, for maximum data rates R, it will be a safe measure to have $R \leq \frac{1}{10\tau_{RMS}}$. If this will not be achieved then the ISI will be significant and the performance of the system degrades. Thus for every system at high data rates, the maximum data rate for transmission can be calculated using this entity, i.e., RMS delay spread. By RMS delay spread, we can determine the coherence bandwidth of the channel which has significant impacts on the performance of the radio system.

2.5 Conclusion

In this chapter two types of the antenna array structures are presented, i.e., an ULA and an UCA. A simplified SC-FDE based system model has been presented. The SC-FDE approach has been considered which is seen to be a good candidate for broadband wireless communication. This scheme shows a better performance and also a better power efficiency since it requires low

PAPR and low IBO requirement for the power amplifier. A channel model for 60 GHz has been discussed and an overview of the different propagation parameters such as path loss, power delay profile, and RMS delay spread is presented. It was seen that the 60 GHz band has high path loss due to absorption feature.

Chapter 3

Antenna Array Considerations

3.1 Introduction

Antenna arrays have been used in a variety of ways to improve the performance of a communication system. Antenna arrays work on the premise that the multipath signals arrive from different directions. The beam pattern of the array is adjusted to lock on to the DOA of the strongest reflection. An antenna array consists of a finite number of elements spatially separated with certain distances. In this report, we utilize the antenna array at the receiver side and then implement beamforming on the received signals. The array receives the LOS as well as NLOS multipath signals. The number of array elements are spatially located to form the arbitrary array geometry. Since we constrain ourself to the ULA and the UCA. Therefore, we want to investigate the required number of array elements M and the inter-element spacing Δ for 60 GHz channels. We will consider the following points.

- The sidelobe/main lobe behavior is dependent on the number of antenna array elements M, inter-element spacing Δ and the antenna array size.
- Using a rectangular window with unity amplitudes, we investigate the impact of physical array parameters on the performance of beamforming for the 60 GHz transceiver system.

This chapter outlines the impact of the physical antenna array parameters such as number of antenna elements M, inter-element spacing Δ on the RMS delay spread and BER in context with 60 GHz. In section 3.2, the impact of the inter-element spacing on the array response will be presented. The derivation for computing the BER is done in section 3.3. In section 3.4, the impact of the physical parameters on the RMS delay spread will

be discussed. Section 3.5, outlines the impact of the array parameters on BER performance. Section 3.6, outlines the beamforming gains with the utilization of the parameters investigated from the simulation results on BER performance. At last, conclusions of the chapter will be presented in section 3.7.

3.2 Impact of Physical Parameters on Antenna Array Beam Pattern

The inter-element spacing Δ between the antenna array elements of the ULA is an important part in designing the ULA [8] and the UCA. It is therefore, necessary to see the effects of varying the physical parameters such as array elements M and inter-element spacing Δ of the ULA and UCA. The simulation for various values of inter-element spacing and fixed number of array elements of the ULA and UCA and also for various numbers of M and fix Δ will be performed in the following subsections.

Impact of Δ on ULA

The impact of varying the inter-element spacing of the ULA can be seen by plotting the spatial responses of the ULA. The spatial responses of the ULA for different values of Δ and for a fixed number of array elements is shown in the Figure 3.1. It is seen from the beam pattern that when the Δ between the antenna array elements is greater than $\lambda/2$, grating lobes appear in the radiation pattern of ULA [9] as can be seen from the Figure 3.1.

It can be proved by examining the equation of the array steering vector of the ULA, $\varphi = e^{j2\pi(\frac{\Delta}{\lambda})\sin(\theta)}$. We know that the $\sin(\theta) \in [-1, 1]$ and from the equation of the array steering vector of the ULA, the exponent term can be $2\pi(\frac{\Delta}{\lambda})\sin(\theta) \in [-2\pi(\frac{\Delta}{\lambda}), 2\pi(\frac{\Delta}{\lambda})]$. Therefore, if $\Delta > \lambda/2$, the exponent term extends beyond $[-\pi, \pi]$ and we can get the peak for several values of θ for the same argument of exponent which causes grating lobes in the array response.

Impact of Δ on UCA

The inter-element spacing and the radius of the UCA are related with each other and the relation is given by the following equation.

$$\Delta = 2R\left(\sin\left(\frac{\pi}{M}\right)\right), \tag{3.1}$$

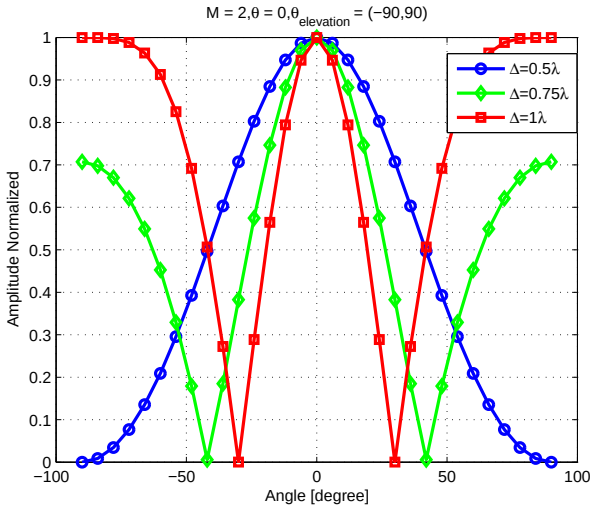

Figure 3.1: Impact of various values of inter-element spacing Δ on beam pattern of ULA $M = 2$.

where R is the radius of the circular array and M is the number of array elements. It is seen from the equation that the radius R and the Δ are related with each other. If we increase the radius, the inter-element spacing will also increase while fixing the number of array elements. The size of the array will also increase for increasing the Δ. The effects of the Δ for a fixed number of array elements can be seen from the beam pattern of the array in the Figure 3.2.

In case of UCA, it is seen that by increasing the inter-element spacing Δ while keeping the number of array elements fixed, it results in a narrower main lobe with high side lobes and on the other hand decreasing the Δ results in an increase of the main lobe width [27]. It is seen from the beam pattern of the receive array that the Δ of UCA is a trade-off between the width of the main lobe and the magnitude of the side lobes [27].

Impact of M on ULA

The simulation is performed for various number of array elements M while keeping the inter-elements spacing $\Delta = 0.5\lambda$ fixed. This results in increasing the size of the array geometry for increasing the array elements. The beam pattern of the ULA shows that for increasing the number of array elements, the beamwidth of the main lobe is getting narrower and the array becomes more directive. By increasing the array elements, side lobes are also introduced but the strength of the side lobes is much less than the main lobe as

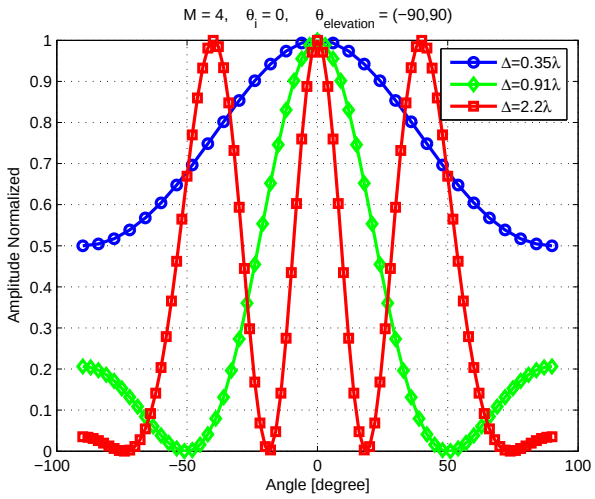

Figure 3.2: Impact of various values of inter-element spacing Δ on beam pattern of UCA.

can be seen from the beam pattern of the ULA in Figure 3.3.

Impact of M on UCA

The beam pattern is plotted for the UCA for various values of M while keeping the R fixed. By fixing the radius R of the UCA and for increasing the array elements M, the size of the array will remain the same while the inter-element spacing will decrease. From the beam pattern of the UCA, it is seen from the Figure 3.4 that the width of the main lobe is not affected by increasing the number of array elements while the strength of the side lobes is decreased.

It is evident from the literature [7, 9, 10, 28] that for good performance of the system with ULA, the inter-element spacing Δ should be equal to half wavelength $\lambda/2$. It is clearly seen from the above simulation results that if the inter-element spacing is greater than half the wavelength for the ULA, then the side lobe strength starts increasing. Therefore, for the case $\Delta \geqslant \lambda$, grating lobes occur which degrade the performance of the system. It can therefore, be concluded the following points from the above simulation plot for ULA and UCA for varying parameters such as Δ and M.

- by increasing the inter-element spacing of the ULA while fixing M, the size of the array will increase which results in introducing the side lobes and for $\Delta \geq \lambda$, grating lobes will occur which results in degrading the performance.

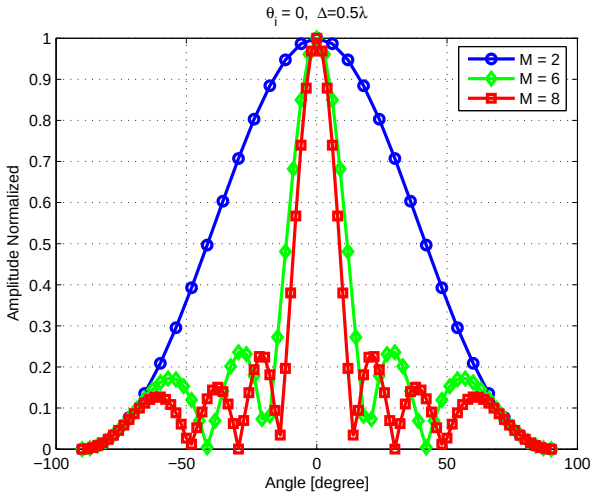

Figure 3.3: Impact of various number of M on beam pattern of ULA.

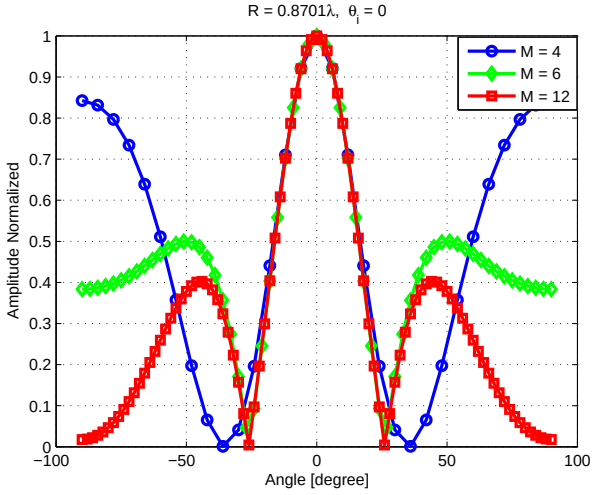

Figure 3.4: Impact of various number of M on beam pattern of UCA.

- by increasing the number of array element M while fixing the Δ of the ULA, the width of the main beam decreases along with side lobes. In this case the strength of the side lobes is much less than the main lobe. In this case also the size of the array increases. It means that the system shows better performance for half the wavelength value of the inter-element spacing.

- for increasing the radius of the UCA, the inter-element spacing Δ will also increase for a fixed number of the array elements $M = 4$. Then the size of the array will also increase which results in decreasing the width of the main lobe along with increasing the strength of the side lobe.

- for increasing the array elements while fixing the radius $R = 0.8701\lambda$ of the UCA will result in decreasing the Δ. In this case the size of the array will remain same. Then the strength of the side lobes will decrease for increasing the M.

On the basis of the above simulation results, the effects of the array parameters will be further analyzed in computing the RMS delay spread and the BER using the 60 GHz channel model after ideal[1] beamforming implementation in Sections 3.4 and 3.5.

3.3 BER Calculation

To assess the performance of a communication system, BER is an important parameter to be considered. Therefore, the BER computation should be done and validated by the simulation results performed in section 3.5. The BER calculation can be derived mathematically. For an AWGN channel,

$$x = s + n, \tag{3.2}$$

where,
s is the BPSK signal having constellation points $-\sqrt{E_b}, +\sqrt{E_b}$, E_b is the symbol energy,
n is the AWGN noise with $\mathcal{N}(0, \delta^2)$, h is the channel impulse response.

Pairwise bit error probability between any two signal points s_m and s_k in AWGN is given as,

[1] *ideal* means that the array is assumed to be steered towards the DOA of the strongest reflection

$$P_b = Q\left(\sqrt{\frac{d^2(s_m, s_k)}{4\delta^2}}\right), \tag{3.3}$$

where, $d^2(s_m, s_k)$ is the Euclidian distance between s_m and s_k. For BPSK, $s_m = +\sqrt{E_b}$ and $s_k = -\sqrt{E_b}$ and the variance $\delta^2 = \frac{N_0}{2}$. The simple BPSK signal constellation is shown in Figure 3.5.

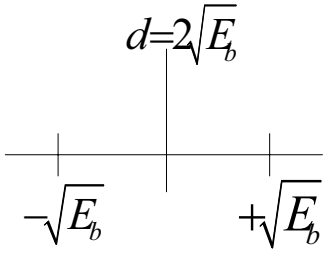

Figure 3.5: BPSK signal constellation.

By substituting the values of $d^2(s_m, s_k)$ and δ^2 in equation (3.3), we get

$$P_b = Q\left(\sqrt{\frac{2E_b}{N_0}}\right), \tag{3.4}$$

For the case of SC-FDE, the signal at the input of the detector is given as,

$$y = s + \widetilde{n}, \tag{3.5}$$

where $\widetilde{n} = \mathcal{F}^{-1}\left(\frac{N}{H}\right)$, $\mathcal{F}^{-1}$ represents the IFFT and $\mathbf{N} = \mathcal{F}(\mathbf{n})$ and $H = \mathcal{F}(h)$. The equation (3.5) is equivalent to time domain finite impulse response (FIR) filter g equals to the inverse of the CIR, i.e., $g = \mathcal{F}^{-1}(\frac{1}{H})$ and $\mathcal{F}$ represent the FFT. Thus equation (3.5) can be equivalently written as,

$$y = s + n * g, \tag{3.6}$$

Let $n' = n * g$. The input and output variance $\delta^2_{n'}$ of the linear system is related as [29],

$$\delta^2_{n'} = \delta^2 \sum_{i=1}^{L} |g_i|^2, \tag{3.7}$$

The conditional probability for the given channel impulse response is given as,

$$P_b\left(\mathcal{E}|\widetilde{h}_1,\widetilde{h}_2,\cdots,\widetilde{h}_L\right)=Q\left(\sqrt{\frac{2E_b}{N_0\sum_{i=1}^{L}|g_i|^2}}\right), \tag{3.8}$$

where $\widetilde{h}_i = h_i\left(t,\theta\right).a\left(\theta\right)$ is the CIR after beamforming and is the i-th multipath component of a given channel realization $\widetilde{h}$ and $h\left(t,\theta\right)$ is the CIR before beamforming. When no beamforming is applied $a\left(\theta\right)=1,\ \forall\theta$ and therefore $\widetilde{h}=h$. The average error probability can thus be computed as,

$$P_b=\int_{\widetilde{h}_L}\cdots\int_{\widetilde{h}_1}P_b\left(\mathcal{E}|\widetilde{h}_1,\widetilde{h}_2,\cdots,\widetilde{h}_L\right)p(\widetilde{h}_1)p(\widetilde{h}_2)\cdots p(\widetilde{h}_L)d\widetilde{h}_1d\widetilde{h}_2\cdots d\widetilde{h}_L, \tag{3.9}$$

where $p\left(\widetilde{h}\right)$ is the probability density function (PDF) of $\widetilde{h}$. The solution of this integral is cumbersome to compute analytically. Therefore, we resort to Monte Carlo based averaging which gives the bit error probability and is given by the following equation.

$$P_b\simeq\frac{1}{N}\sum_{i=1}^{N}P_b\left(\mathcal{E}|\widetilde{h}_1^i,\widetilde{h}_2^i,\cdots,\widetilde{h}_L^i\right), \tag{3.10}$$

where N is the number of channel realization. The BER is analyzed using the equation (3.10). Figure 3.6, shows the comparison of BER with analytical simulation without beamforming in LOS and NLOS scenarios. The BER performance is computed by selecting the various values of the SNR in decibel (dB). The simulation parameters are given in the Table 3.1.

Parameters	Values
Data length	1024
FFT length	1024
CP length	100
Number of simulation	40000
Channel environment	LOS/NLOS
Sampling rate	2 GHz
Tx/Rx separation d	1 m

Table 3.1: Simulation parameters for BER without beamforming.

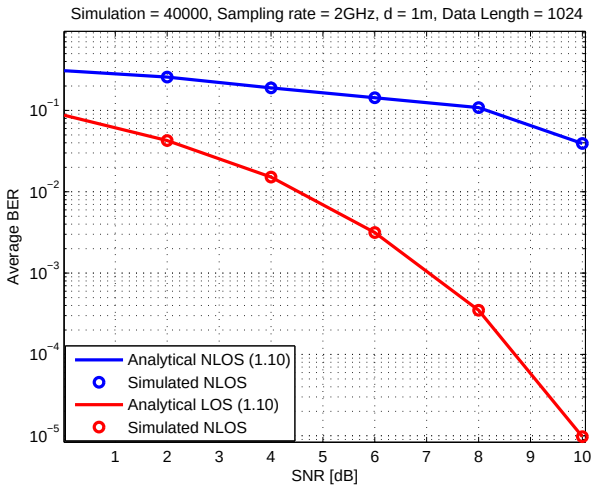

Figure 3.6: Comparison analytical and simulated BER without beamforming.

3.4 Impact of Physical Parameters on RMS Delay Spread

The 60 GHz channel suffers from RMS delay spread. This effect of RMS delay spread can be greatly reduced by using the antenna array with beamforming implementation. In this scheme, it is assumed that the DOA of all the multipath are known and we steer the array towards the strongest path. The improvement can be seen by plotting the RMS delay spread for various values of the physical parameters of the antenna array such as antenna elements M and inter-element spacing Δ of the ULA and the UCA. The improvement in RMS delay spread has been investigated and is analyzed using the equation (3.10) for the 60 GHz channel model. The investigation was done for various physical parameters of the antenna arrays, i.e., ULA and UCA. For each channel realization, we compute the RMS delay spread and then average over all the realizations. The system parameters for the simulation are given in Table 3.2. Throughout this chapter these parameters will be considered for the case of ULA and UCA geometries. The 60 GHz channel model is taken from [20]. The simulation is done by varying one of the antenna array parameter and all other parameters fixed. The value of Δ and R are taken as the multiple of signal wavelength λ.

Parameters	Values
Data length	1024
FFT length	1024
CP length	100
Number of simulation	20000
Channel environment	LOS/NLOS
Sampling rate	2 GHz
Tx/Rx separation d	1 m

Table 3.2: Simulation parameters for 60 GHz channel.

3.4.1 Impact of M on ULA

The simulation is performed for various number of ULA elements M while keeping fixed the inter-element spacing Δ. By this selection the size of the array geometry will increase which affects the beam pattern as is explained in section 3.2. It means width of the main beam decreased along with side lobes. The array becomes directive and this suppresses the multipath. The simulation results for the ULA geometry are shown in Figures 3.7 and 3.8, respectively in LOS and NLOS scenarios. It is seen from the Figure 3.7 that average RMS delay spread improves after the beamforming implementation. By increasing the number of array elements, the array beamwidth keeps on getting narrower with increasing M and the array becomes more directive. Therefore, it looks towards a specific DOA of the strongest reflection. This greatly reduced the multipath effect from different directions.

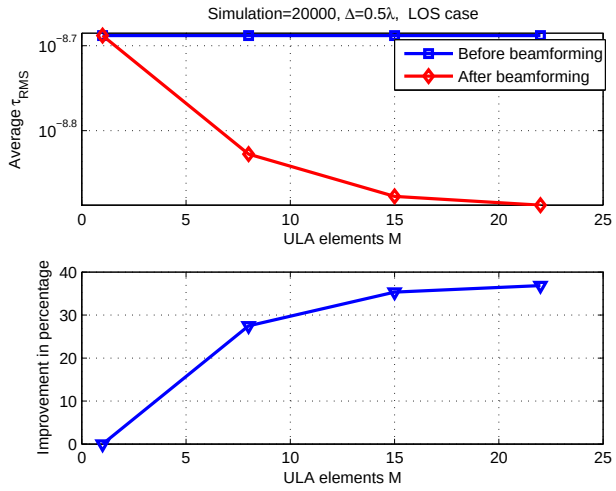

Figure 3.7: Impact of ULA M on average τ_{RMS} in LOS case for $\Delta = 0.5\lambda$.

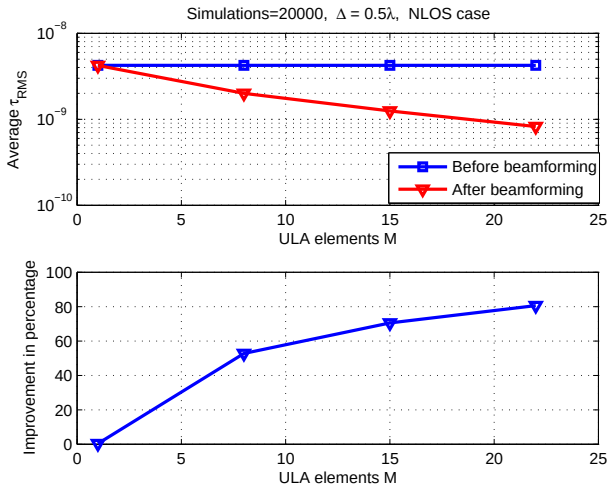

Figure 3.8: Impact of ULA M on average τ_{RMS} in NLOS case for $\Delta = 0.5\lambda$.

The second subplot of Figures 3.7 and 3.8, show the improvement in RMS delay spread in terms of percentage in LOS and NLOS scenarios using the ULA geometry. The improvement in percentage has been calculated by using the following equation as,

$$Percent = 100 \times \left[\frac{abs(\varsigma_{WBF} - \varsigma_{WOBF})}{(\varsigma_{WOBF})} \right] \tag{3.11}$$

where ς_{WBF} denotes the value of the average RMS delay spread τ_{RMS} after the beamforming implementation and ς_{WOBF} denotes the value of the average RMS delay spread τ_{RMS} before the implementation of beamforming. The improvement in RMS delay spread for various number of antenna elements M in both LOS and NLOS cases can be seen from Tables 3.3 and 3.4. It is noted that the improvement for the first eight elements is much greater than the improvement for further increasing the array elements M for NLOS case. As is seen from the simulation results that the improvement in BER for LOS case is not significant.

Number of Antenna Elements M	Improvement in Percentage
1 to 8	26
8 to 16	8
16 to 22	4

Table 3.3: Improvement in RMS delay spread with increasing M at $\Delta = 0.5\lambda$ in LOS case.

Number of Antenna Elements M	Improvement in Percentage
1 to 8	50
8 to 16	20
16 to 22	10

Table 3.4: Improvement in RMS delay spread with increasing M at $\Delta = 0.5\lambda$ in NLOS case.

The improvement for NLOS case is 24 percent more than for the LOS case with the same number of array elements. It is seen from the simulation result that the RMS delay spread improves upto an eight number of array elements in LOS case although the improvement is not much better. The improvement in RMS delay spread becomes insignificant by further increasing the array elements as can be seen from the second subplot of the Figures 3.7 and 3.8, in LOS and NLOS scenarios using the ULA geometry. It is evident that the system shows better performance in terms of τ_{RMS} by increasing the array elements M. However, the computational complexity and the implementation cost will also increase with increasing the array elements M. Therefore, we can conclude that the array elements M are the trade-off between the computational complexity and the performance.

3.4.2 Impact of Δ on ULA

The simulation is done for various values of Δ with eight ULA elements. For fixing the number of array elements M and increasing the value of Δ, the size of the array will increase which affects the beam pattern of the array. This effect of an increase in size of the array geometry has been discussed in section 3.2. Figures 3.9 and 3.10, show the effect of inter-element spacing Δ on the RMS delay spread in LOS/NLOS scenarios. It is seen from the Figure 3.9 that by increasing the value of Δ, the RMS delay spread improves accordingly for the LOS case. However, it is noted that the RMS delay spread improves upto an optimum value of the Δ which is the half wavelength value, i.e., 0.5λ. For further increasing the value of Δ, the improvement is decreased as is seen clearly from Figure 3.9. This improvement in RMS delay spread can be seen from the second subplot of Figure 3.9 and is computed in terms of percentage using the equation (3.11). It is evident that the RMS delay spread improves upto 20 percent for 0.5λ inter-element spacing Δ. Although the improvement is not significant by which we can say that the inter-element spacing has not much effect on the RMS delay spread for the LOS case.

Figure 3.10, shows the impact of inter-element spacing Δ on the RMS delay spread in NLOS case. It is seen that the RMS delay spread improves

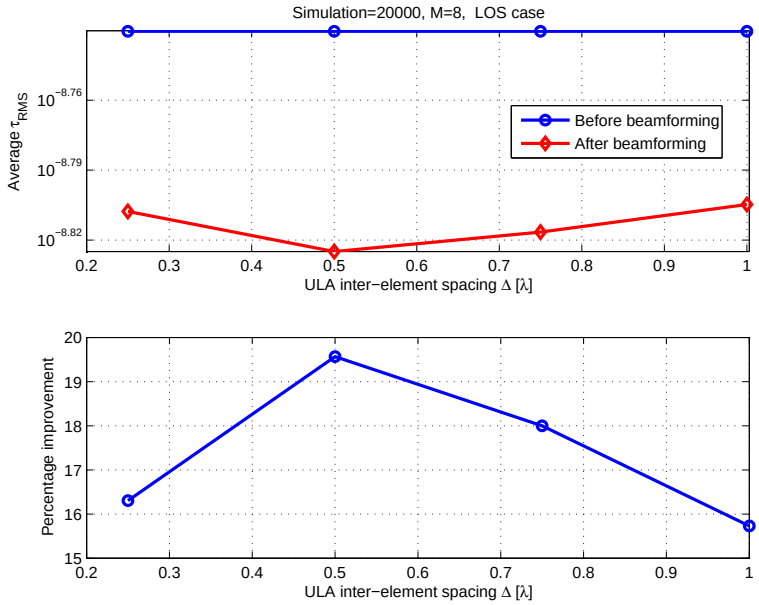

Figure 3.9: Impact of ULA Δ on average τ_{RMS} in LOS case for $M = 8$.

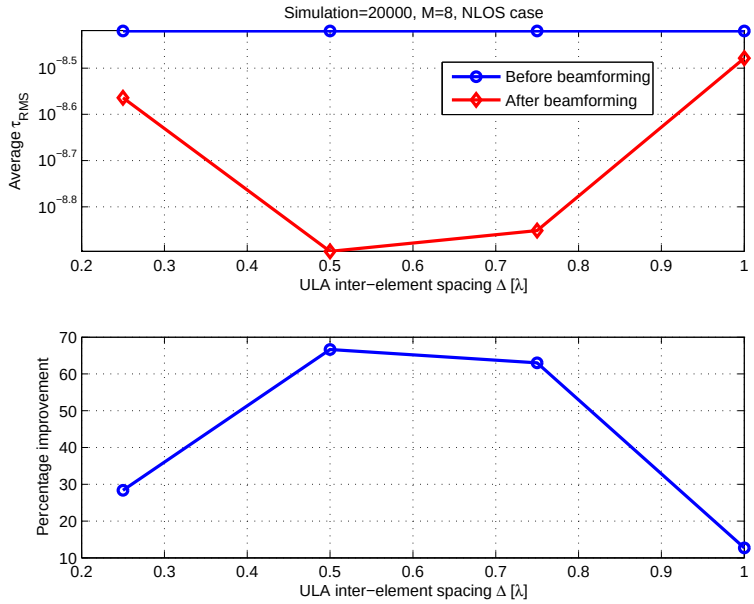

Figure 3.10: Impact of ULA Δ on average τ_{RMS} in NLOS case for $M = 8$.

upto an optimum value of the inter-element spacing Δ in NLOS case which is the half wavelength value. However, the improvement in this case is better than the one for LOS case but again we see that the improvement is not significant. In this case, it shows 45 percent more improvement in RMS delay spread as can be seen from the second subplot of Figure 3.10. The RMS delay spread improves upto the optimum value and then start decreasing. The effect of increasing the value of Δ has been explained in section 3.2.

The effect of changing the value of Δ has been reported in [9,28]. Since by increasing the inter-element spacing Δ, the height of the side lobes increases and grating lobes occur for $\Delta \geq \lambda$ as is reported in [9]. The occurrence of the grating lobes depends upon the array inter-element spacing Δ. According to [9, 28], the grating lobes can be avoided in an array antenna if the inter-element spacing Δ is restricted to $\Delta \leq \frac{\lambda}{2}$.

3.4.3 Impact of M on UCA

For the case of UCA, the simulation is performed for various numbers of array elements by keeping the radius R fixed. By increasing the number of array elements and fixing R, the size of the array will not change. But the inter-element spacing decreases for increasing M. The effects of varying the array elements and the inter-element spacing of the UCA are shown in the Figures 3.11 and 3.12 respectively for the LOS and NLOS scenarios. It is clearly seen from the second subplots of the Figures 3.11 and 3.12, that the RMS delay spread τ_{RMS} improves by increasing the number of UCA elements for LOS and NLOS case after the implementation of beamforming. It is noted that the improvement is significant by increasing the number of UCA elements for LOS case.

Number of Antenna Elements M	Improvement in Percentage
4 to 8	42
8 to 12	8
12 to 16	4
16 to 20	2

Table 3.5: Improvement in RMS delay spread with increasing M in LOS case.

The improvement can be seen clearly from the Tables 3.5 and 3.6 in LOS/NLOS case. This follows that the improvement for the first eight element is better than for further increasing the array elements. This effect is done, as we have seen from the simulation plots in section 3.2 that for increasing the array elements while keeping the radius fixed, the array beamwidth

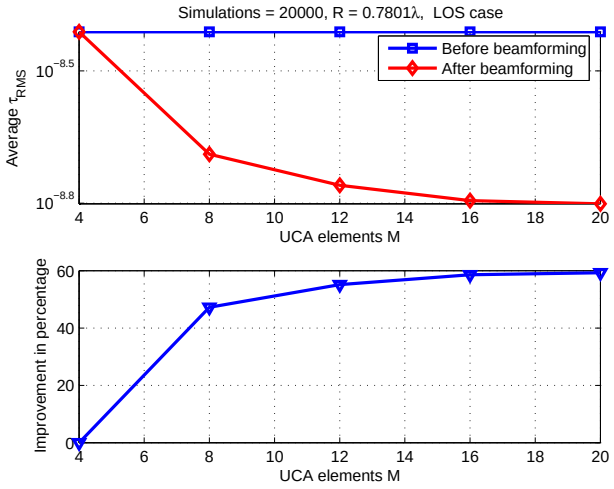

Figure 3.11: Impact of UCA M on average τ_{RMS} in LOS case.

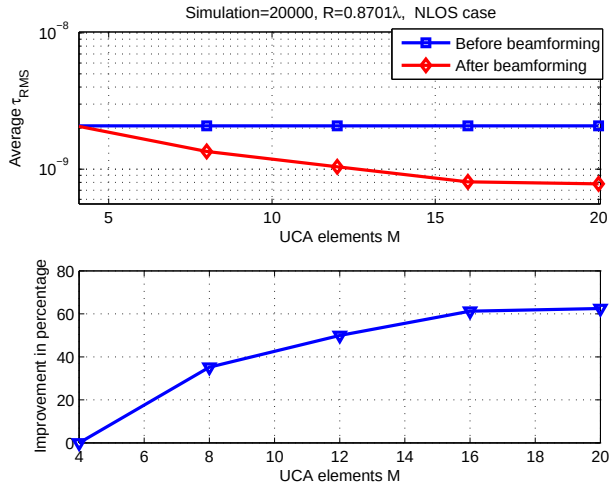

Figure 3.12: Impact of UCA M on average τ_{RMS} in NLOS case.

Number of Antenna Elements M	Improvement in Percentage
4 to 8	38
8 to 12	12
12 to 16	10
16 to 20	4

Table 3.6: Improvement in RMS delay spread with increasing M in NLOS case.

becomes narrower for the first eight elements and then for further increasing the element, the beamwidth is not much decreased since the size of the array remains fixed. Also the increment in the number of elements controls the strength of the side lobes. The beamwidth of the main beam is controlled by the size of the antenna arrays. The side lobe will introduced with increasing the number of array elements but the strength of the side lobes is very low as compared to the main lobe. The narrower the beamwidth, the more directive the antenna array will be. Therefore, by more antenna array elements, the array becomes more directive [8, 22] which results in the improvement of the RMS delay spread.

3.4.4 Impact of Δ on UCA

The simulation is performed for various values of R while keeping the array elements fixed. The increment of R will result in an increment of the Δ which increases the size of the array. Then for increasing Δ for a fixed number of array elements, the beamwidth of the main lobe will getting on narrower and the strength of the side lobes increases. This will degrade the performance of the system with increasing the value of Δ. Figure 3.13 shows the impact of increasing the Δ of the UCA. It is seen that initially the RMS delay spread improves and then this improvement starts decreasing by increasing the Δ of the UCA. This happens because by increasing the Δ, the width of the main lobe decreases while the height of the side lobes increases as shown in the Figure 3.2. This effect of increasing the Δ of UCA on the RMS delay spread in percentages can be computed by using equation (3.11) and the effect can be seen in the second subplot of Figures 3.13 and 3.14 in both LOS and NLOS scenarios.

The plots are provided by giving the values of the radius of the UCA and the inter-element spacing of the UCA can be calculated using equation (3.1) and this is done throughout the chapter. Since it can be seen from the simulation results that for $\Delta > 0.66\lambda$, the improvement in RMS delay spread starts decreasing. Therefore, we can conclude in considering the simulation results obtained, that for a better performance in RMS delay spread, the value for Δ at $R = 0.8701\lambda$ will be the 0.66λ. From the simulation results, it is seen that the average RMS delay spread improves 22 percent at $\Delta = 0.66\lambda$ in LOS case and 50 percent in NLOS case. From the simulation results, it is also noted that the improvement is insignificant in both cases LOS/NLOS.

The impact of the physical parameters show an improvement in RMS delay spread of the 60 GHz as can be seen from the simulations. It is clearly seen from the plots that the RMS delay spread is improved as the number of array elements M are increased for an optimum value of the inter-element

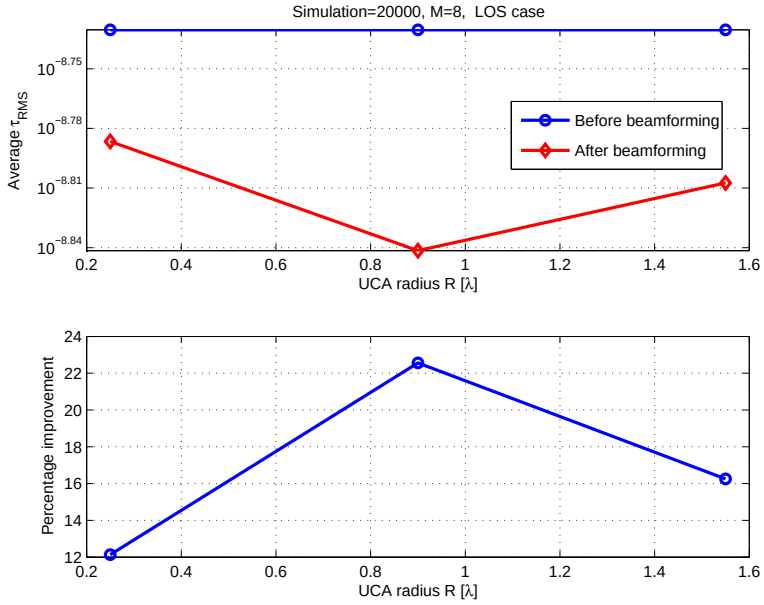

Figure 3.13: Impact of UCA R on average τ_{RMS} in LOS case.

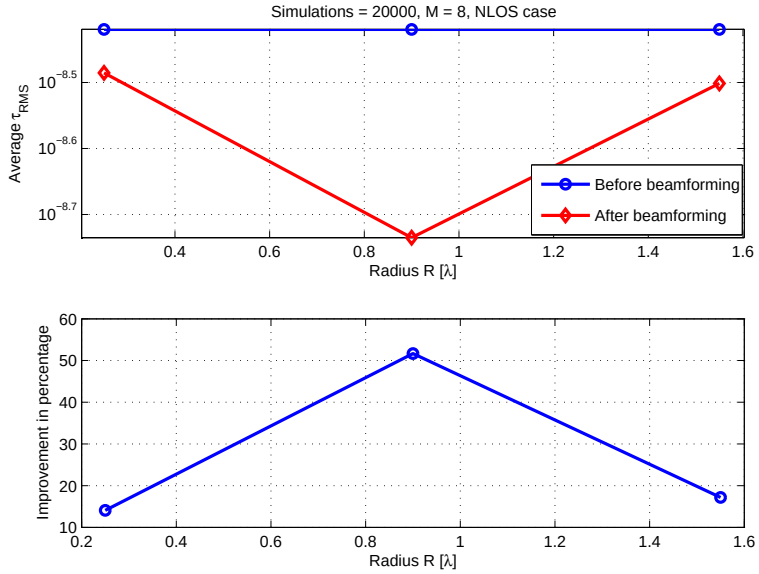

Figure 3.14: Impact of UCA R on average τ_{RMS} in NLOS case.

spacing Δ of the ULA and the UCA in LOS/NLOS scenarios. This happens because by increasing the number of the antenna array elements the beamwidth becomes narrower and the steering of the array becomes more directive [22]. It can be concluded that the number of array elements M are the trade-off between the computational complexity and the performance. Therefore, in considering the trade-off, we can use an eight number of array elements with an optimum value of 0.5λ of Δ for ULA and 0.66λ for UCA.

3.5 Impact of physical parameters on the BER

In assessing the performance of a communication system, the BER is considered to be an important parameter. It is therefore required to see the effects of varying the physical parameters of the array on the BER of the system. The BER performance has been evaluated using the 60 GHz channel model [20] with multipath fading in LOS/NLOS scenarios. The SC-FDE signal model presented in chapter 2, is analyzed using the equation (3.10). For each channel realization, we compute the BER and then average over all the realizations. The results are plotted against the number of antenna elements M, inter-element spacing Δ of the ULA and the UCA. The simulation parameters are the same as given in Table 3.2.

3.5.1 Impact of M on ULA

The impact of various number of the ULA elements M on the BER in LOS and NLOS scenarios are shown in the Figures 3.15 and 3.16 respectively. The simulation is performed for various number of array elements while keeping the value of inter-element spacing Δ fixed. It is seen from the Figure 3.15 that the BER performance improves significantly upto a certain number of array elements after the implementation of the beamforming. It is seen that upto a number of array elements eight, the average BER performance is improved significantly. For further increasing the array elements, the improvement is not significant. The improvement of the average BER in percentage can be seen from the Tables 3.7 and 3.8 in LOS/NLOS case. The improvement of the averaged BER in percentage can be calculated by using the following equation.

$$Percent = 100 \times \left[\frac{abs(\Upsilon_{WBF} - \Upsilon_{WOBF})}{(\Upsilon_{WOBF})} \right] \tag{3.12}$$

where Υ_{WBF} denotes the value of the average BER after the beamforming implementation and Υ_{WOBF} denotes the value of the average BER before

the implementation of beamforming.

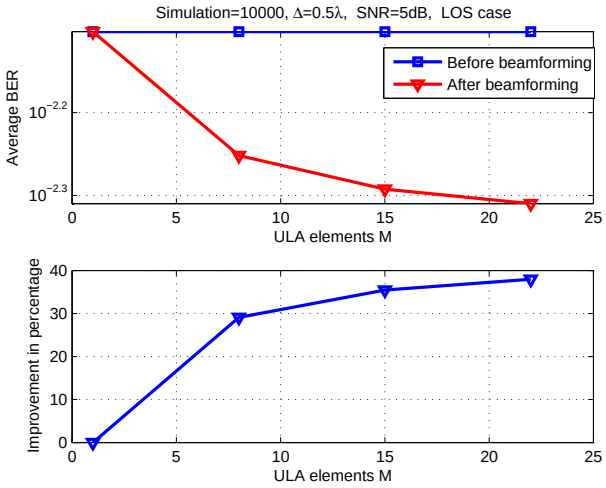

Figure 3.15: Impact of ULA M on average BER in LOS case.

Number of Antenna Elements M	Improvement in Percentage
1 to 8	28
8 to 16	6
16 to 22	4

Table 3.7: Improvement in average BER with increasing M at $\Delta = 0.5\lambda$ in LOS case.

It is noted from the Tables 3.7 and 3.8 that the improvement for the first eight elements is much greater than the improvement for further increasing the array elements M. Figure 3.16, shows the improvement of the BER in NLOS case. It is also noted that the improvement in BER for the NLOS case is better as compared to the LOS case. This effect of improving the BER by increasing the array elements is because array beamwidth becomes narrower and thus the array becomes more directive by increasing the number of array elements. However, the side lobes also appeared for increasing the array elements but the strength of the side lobes is much less as compared to the main lobe.

3.5.2 Impact of Δ on ULA

The effects of inter-element spacing on the BER performance are plotted in Figures 3.17 and 3.18 for the LOS/NLOS scenarios. The simulation parame-

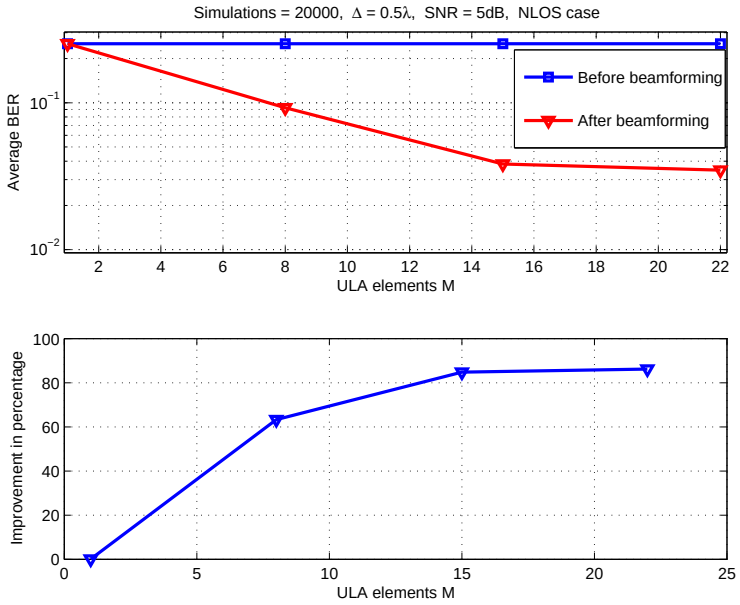

Figure 3.16: Impact of ULA M on average BER in NLOS case.

Number of Antenna Elements M	Improvement in Percentage
1 to 8	60
8 to 16	20
16 to 22	9

Table 3.8: Improvement in average BER with increasing M at $\Delta = 0.5\lambda$ in NLOS case.

ters are the same as given in Table 3.2. We vary the Δ for $M = 8$. From the Figure 3.17, it is clearly seen that by increasing the inter-elements spacing Δ for the case of ULA, the BER improves significantly, i.e., 45 percent for the half wavelength 0.5λ. However, this improvement is increased upto an optimum value of the Δ and then starts going to decrease for the value of Δ greater than the half wavelength 0.5λ. This effect of inter-element spacing on the array beam pattern has been discussed in section 3.2. The optimum value of the Δ is to be noted as 0.5λ which is also reported in [9, 28].

Figure 3.18, shows the improvement in BER by increasing the inter-element spacing in NLOS case. It is also noted the improvement in BER for NLOS case is 80 percent for the half wavelength 0.5λ. However, in the NLOS case, the improvement is noted to be 35 percent more than the one obtained in LOS case for half wavelength 0.5λ of the inter-element spacing

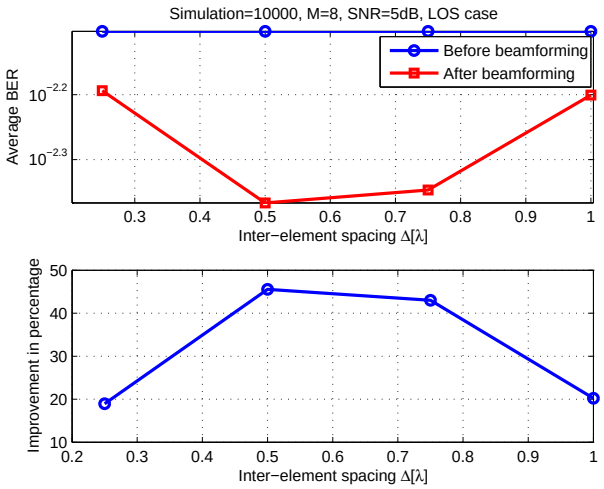

Figure 3.17: Impact of ULA Δ on average BER in LOS case.

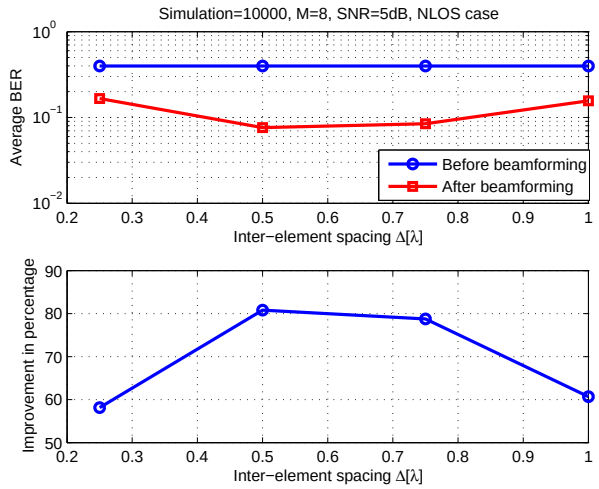

Figure 3.18: Impact of ULA Δ on average BER in NLOS case.

Δ. From the above simulation results, it is noted that the improvement is not much significant in NLOS case by increasing the Δ.

3.5.3 Impact of M on UCA

In case of UCA, the simulation results are plotted for various numbers of array elements M for the LOS and NLOS scenarios, as shown in the Figures 3.19 and 3.20, respectively. The array radius will remain fixed while with

increasing the M, the Δ will vary accordingly. From the subplots of the Figures 3.19 and 3.20, it is clearly seen that the BER improves by increasing the number of UCA antenna elements after the implementation of the beamforming for the LOS and NLOS case. The improvement of the BER by increasing the array elements M for LOS and NLOS cases in terms of percentage can be computed by using equation (3.12). The effect of increasing the M on the beam pattern of the array has been explained in section 3.2. The percentage improvements are given in Tables 3.9 and 3.10 for both the LOS and NLOS cases. This improvement becomes insignificant for further increasing the array elements. It is noted from the simulation results that the improvement for the first eight elements is much greater than the improvement for the elements from 8 to 16 and so on for the LOS case.

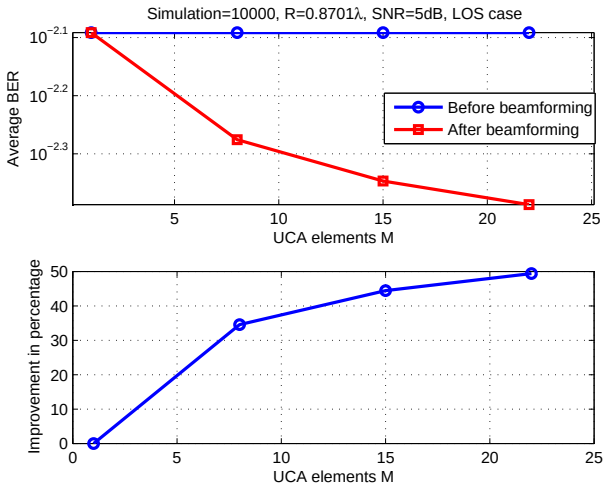

Figure 3.19: Impact of UCA M on average BER in LOS case.

Number of Antenna Elements M	Improvement in Percentage
1 to 8	35
8 to 16	10
16 to 22	5

Table 3.9: Improvement in average BER with increasing UCA M in LOS case.

But in the NLOS case as shown in Figure 3.20, the BER improves significantly upto an eight number of array elements, i.e., 70 percent and then for further increasing the number of array elements, i.e., from 8 to 16 the

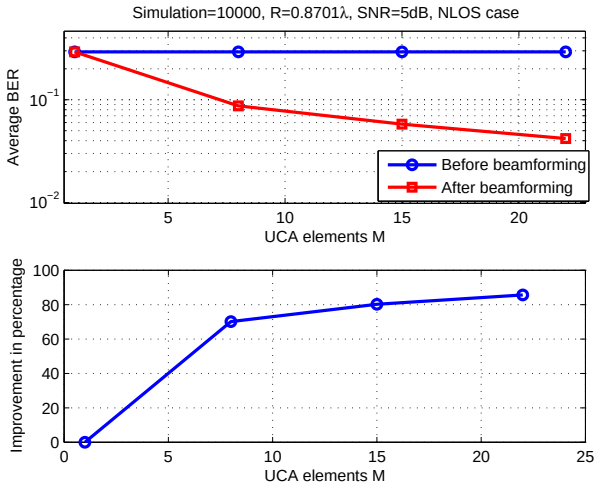

Figure 3.20: Impact of UCA M on average BER in NLOS case.

Number of Antenna Elements M	Improvement in Percentage
1 to 8	70
8 to 16	10
16 to 22	5

Table 3.10: Improvement in average BER with increasing UCA M in NLOS case.

improvement is much less than the one for the first eight elements. This improvement has been computed in percentage by using the equation (3.12) and can be seen from the second subplots of Figures 3.19 and 3.20 respectively.

3.5.4 Impact of Δ on UCA

The simulation is performed for various values of inter-element spacing Δ of the UCA by keeping the array elements M fixed. The inter-element spacing Δ is related with R of the UCA by the equation (3.1). If we increase the Δ, the radius of the UCA will increase, which results in increasing the size of the UCA. The effects of varying the Δ of the UCA in LOS and NLOS scenarios for a number of array elements of 8 can be seen in Figures 3.21 and 3.22 respectively. It is seen from Figure 3.21 that the BER improves by increasing the Δ of the UCA in LOS case. This improvement is better for optimum values of R and Δ that can be seen from the plot as $R = 0.8701\lambda$ and $\Delta = 0.66\lambda$, i.e., 50 percent. By further increasing the Δ, the improvement is decreased. The improvement in percentage can be seen from the Figure 3.22

for the UCA in NLOS case which is 85 percent. The optimum value of Δ for this case is noted as 0.66λ then for further increasing the Δ, improvement in BER starts to decrease. However, the BER improves much better in NLOS case as compared to the LOS case.

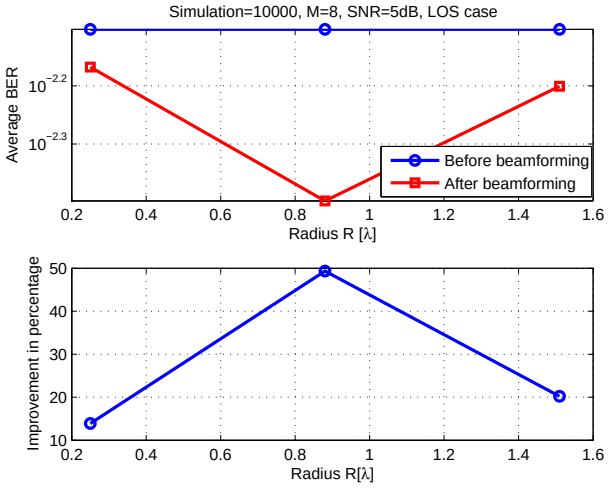

Figure 3.21: Impact of UCA R on average BER in LOS case.

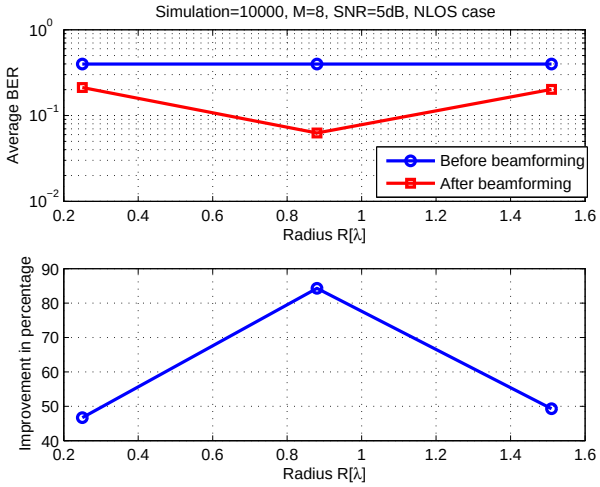

Figure 3.22: Impact of UCA R on average BER in NLOS case.

3.6 Beamforming Gains at 60 GHz

The BER has been computed by using the equation (3.10) for the 60 GHz channel model. The BER performance is computed by selecting the various values of the SNR in decibel (dB). The simulation is performed for $M = 8$, the optimum value of the inter-elements spacing Δ of the ULA and the UCA which are investigated in the above experiments performed for the BER computation. The simulation parameters for the ULA and UCA are given in Table 3.11. For each channel realization, we compute the BER and then average over all the channel realizations. The results are plotted against the SNR for the ULA and the UCA. The simulation was performed for the 60 GHz channel model and the effects of utilizing the physical parameter with ideal beamforming implementation, on the BER were investigated. It is seen from the Figures 3.23, that the BER improves after the beamforming implementation with selected parameters.

Parameters	Values
Data length	1024
FFT length	1024
CP length	100
Number of simulation	20000
Number of element	8
Inter-element spacing of ULA	0.5λ
Inter-element spacing of UCA	0.66λ
Channel environment	LOS/NLOS
Sampling rate	2 GHz
Tx/Rx separation d	1 m

Table 3.11: Simulation parameters for 60 GHz channel.

It is clearly seen from the Figures 3.23 that the average BER improves by using the optimum parameters investigated from the simulation results in the above experiments. The improvement in case of NLOS is significant while for LOS case, it is comparable to that without beamforming.

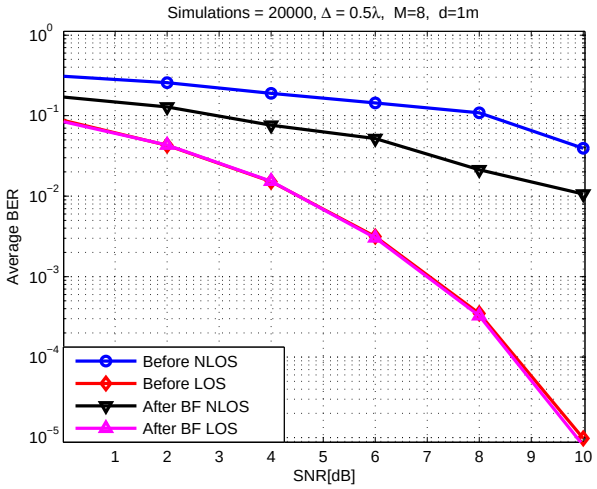

Figure 3.23: Beamforming gains at 60 GHz using ULA.

3.7 Conclusion

In this chapter, we derived the analytical approach for computing the BER which was verified with Monte Carlo simulations. From the above simulation results, it can be concluded that the physical parameters of the ULA and the UCA show great impact on the RMS delay spread and the BER performance. The optimum value of radius of the UCA and the inter-element spacing of the ULA show a significant improvement in the RMS delay spread and the BER of the 60 GHz transceiver system. From the simulation results, it is seen that for implementing the beamforming for 60 GHz using the ULA and UCA, the optimum values of the Δ are 0.5λ and 0.66λ respectively. It is seen that the radius of UCA is channel dependent as seen from different value for R in LOS and NLOS case in calculating the BER. The increasing number of antenna elements provide better improvement in RMS delay spread and in BER for the 60 GHz channel. However, by increasing the number of antenna array element, the implementation complexity will increase. It is therefore concluded that the array elements are the trade-off between the computational complexity and the performance. It is seen from the experiments that by using the arrays with the utilization of the beamforming, the problems of the 60 GHz channel such as RMS delay spread and ISI are greatly reduced.

Chapter 4

Beamforming at 60 GHz

4.1 Introduction

In this chapter, we introduce a novel approach of signal combining at RF level. Since in the conventional system, the signal combining is done after the digital down conversion (DDC) of the RF signal. The conventional beamforming schemes require two ADCs and two mixers for each antenna element which make the scheme difficult to realize, especially when a large number of antenna elements are required and when the sampling frequency is in the range of Gsps. In the proposed scheme, we do the combining of the signals at RF level which is simple hardware wise. The motivation and the problem definition is presented in section 4.2. The proposed beamforming algorithm will be explained in section 4.3. The performance of the proposed scheme in terms of BER is presented in section 4.4. The beamforming gains at the 60 GHz with the implementation of the proposed beamforming algorithm with utilizing of the investigated physical parameters of the antenna arrays will be presented in section 4.5. The effect of the scanning angle step size will be provided in section 4.6. At last the conclusions of the chapter are presented in section 4.7

4.2 Motivation and Problem Definition

In conventional beamforming schemes, the signal combining is done in the digital domain. Numerous classical beamforming algorithms such as multiple signal classification (MUSIC), estimation of signal parameter via rotational invariance techniques (ESPRIT) and many others mentioned in [15,19,30,31], are used for the beamforming in conventional system. Each beamforming algorithm have its own advantages and disadvantages in terms of computa-

tional complexity and performance. The detailed description of each of the conventional beamforming algorithms can be found in [7,9,11,32]. The block diagram of the conventional beamforming architecture is shown in Figure 4.1. It is seen from the block diagram that two mixers and two ADCs are used for each antenna element. This shows that the implementation of this scheme becomes complex and expensive for large number of array elements. This approach also shows several advantages such as more flexibility and more accuracy. However, it also has some disadvantages:

- It requires two ADCs and two mixers for each antenna which increases the cost of the scheme and the scheme is also power inefficient due to the high power consumption of the ADCs.
- Its computational complexity is very high which makes the scheme difficult to implement.

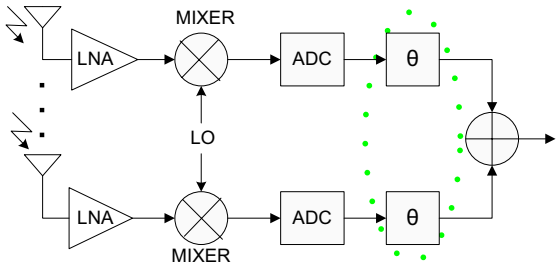

Figure 4.1: Block diagram of conventional beamforming.

Therefore, the crucial points in designing the beamforming scheme, are the complexity, robustness and power dissipation. The power consumption of the ADC is directly proportional to the sampling frequency which is in GHz for the 60 GHz transceiver system. The antenna size for the 60 GHz is very small. Therefore, if we put more antenna elements along with ADCs for the beamforming implementation, this will increase the circuit complexity and the power consumption. Therefore, the conventional beamforming architecture when used with 60 GHz doesn't support low cost, low power devices. Therefore, another approach has been proposed in order to reduce the computational complexity and the implementation cost [13] which is the main motivation behind this work.

The basic block diagram of the proposed approach is shown in Figure 4.2. In this approach the signal combining is done at RF level. Therefore, it is difficult to implement conventional beamforming algorithms (MUSIC and ESPRIT), using this scheme. Since the classical beamforming approaches

require in-phase/quadrature phase (I/Q) channel per antenna element, which in this case is not available. Because in the proposed scheme, the signal combining is done at RF level where, no I/Q is present. It is also seen from the block diagram that the proposed beamforming scheme needs only one mixer and one ADC for the complete antenna array system. There are some important advantages of this approach mentioned below which make it suitable for 60 GHz.

- the signal combining at the RF level makes the approach hardware wise less complex.
- since it requires only one mixer and one ADC, which makes this approach less expensive.
- because of one mixer and one ADC, the power dissipation as compared to the conventional approach will be greatly reduced.

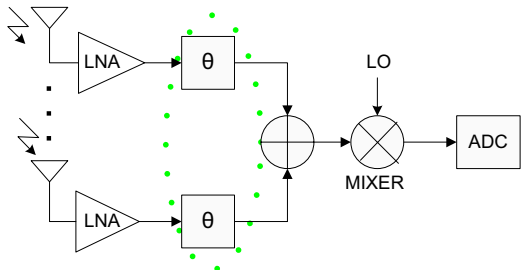

Figure 4.2: Proposed beamforming.

4.3 Beamforming Algorithm

We propose a beamforming solution for the 60 GHz beamforming architecture as shown in Figure 4.2. The flow chart of the proposed beamforming algorithm is given in Figure 4.3. We propose a hardware wise low complexity beamforming algorithm in which beam forming is done at RF level. The beamforming algorithm is explained step-wise as can be seen from the flow chart.

4.3.1 Initialization

The first step is the initialization step in which we initialize the scanning angle to a fixed value of angle θ, i.e., θ_0 and then introduce a step size θ_Δ

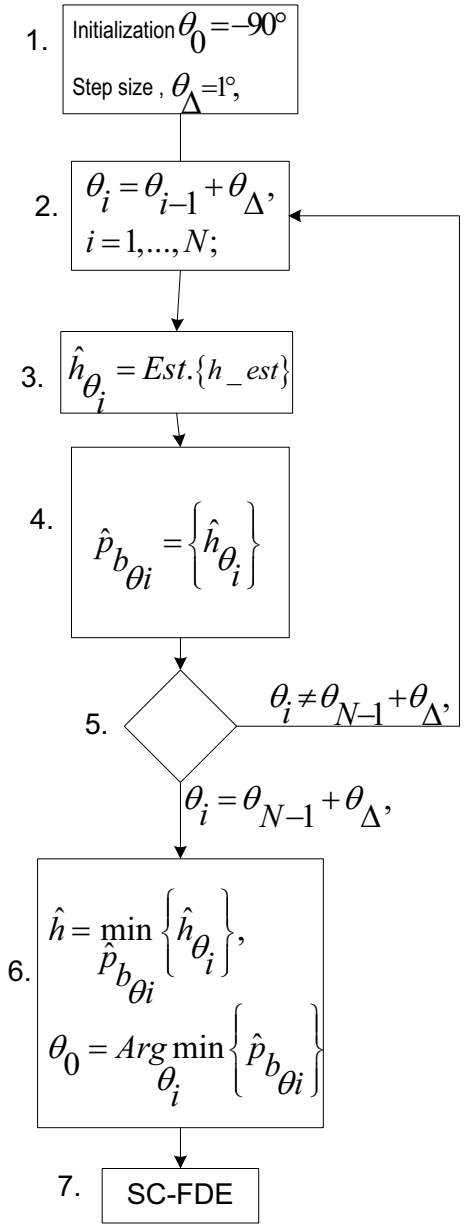

Figure 4.3: Beamforming algorithm flow chart.

for the array scanning range. Then we initialize the scanning range θ_i for the elevation angle of the array steering vector $a(\theta, \theta_i)$. We consider the elevation angle only in the scanning range and assume the azimuth angle equal to zero. The ULA and UCA scans the channel for the whole range of elevation angles. The array steering vector for the ULA and UCA with M equally spaced elements can be given by the following equation [19].

$$a(\theta) = \sum_{m=1}^{M} e^{j\left(\frac{2\pi m\Delta}{\lambda}(\sin(\theta))\right)}, \tag{4.1}$$

$$a(\theta, \varphi) = \sum_{m=1}^{M} e^{j(\cos(\varphi_i - \varphi_m)\sin(\theta_i) - \kappa a\cos(\varphi - \varphi_m)\sin(\theta))} \tag{4.2}$$

where $\kappa = \frac{2\pi}{\lambda}$, a is the radius of the UCA array, θ_i is the elevation angle and φ_i is the azimuth angle where the array should be steered. The scanning step size has great impact on the performance of the system. Since, if the scanning step size is large then the computational complexity will be low, with the expense of performance of the system. Therefore, the scanning step size is the trade-off between the computational complexity and the performance. The array starts scanning the channel with $\theta_0 = -90°$ and in a step size of $\theta_\Delta = 1°$ for the whole range of elevation angles, i.e., (−90°,90°). The scanning for each angle can be represented by the following equation in second step of the flow chart.

$$\theta_i = \theta_{i-1} + \theta_\Delta, \tag{4.3}$$

where θ_i is the scanning angle and $i = 1, 2, \cdots, N$, N is the total number of scanning steps in the elevation angle and θ_Δ is the scanning step size. The effect of the scanning step size can be seen in Figures 4.4 and 4.5 and is also explained for 60 GHz in [13]. It is seen from the plots that if the step size is 1°, then it will cover the maximum multipath direction but if the step size is 20°, then it effects the coverage for the multipath coming from 10°.

4.3.2 Channel Estimation

In the third step, we receive the channel impulse response h_{θ_i}, when the array is steered in the direction θ_i. We estimate the channel in the direction θ_i, which gives us $\hat{h}_{\theta_i}$. We do this step for the LOS/NLOS scenarios. The perfect CSI is considered in the algorithm. Different techniques such as pilot symbol assisted modulation (PSAM), minimum mean square error (MMSE) and least mean square (LMS) can also be used for the channel estimation. For the

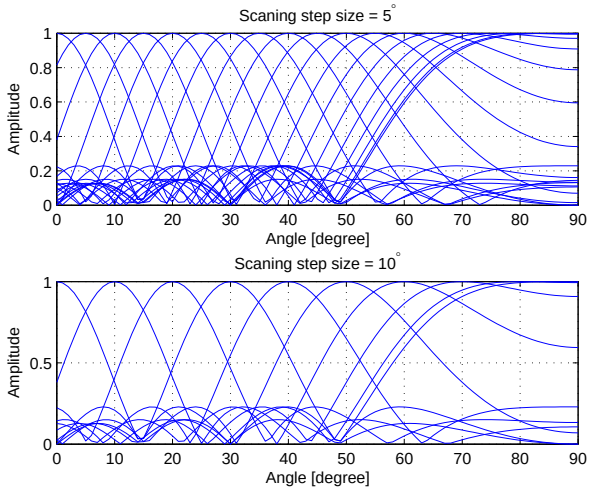

Figure 4.4: Scanning step size of 5° and 10°, $M = 8$, $\Delta = 0.5\lambda$ of ULA.

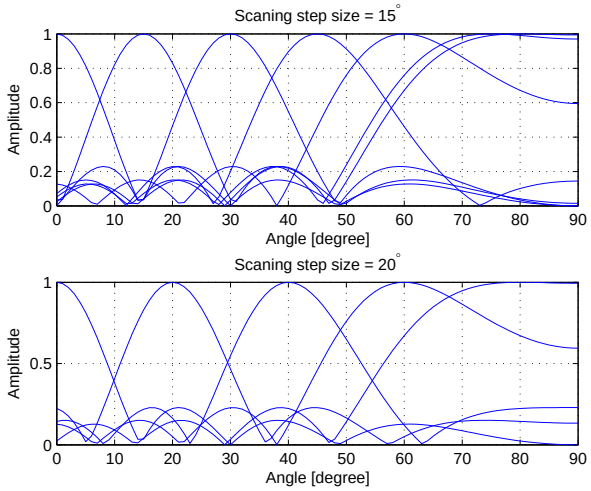

Figure 4.5: Scanning step size of 15° and 20°, $M = 8$, $\Delta = 0.5\lambda$ of ULA.

PSAM scheme [33], the channel can be estimated by periodically inserting the pilot symbols within the data frame. The quality of the channel estimates depends on the number of pilot symbols. If sufficient number of symbols are inserted, the channel can be perfectly estimated. The detailed description of PSAM can be found in [34]. According to [35], in a high-delay spread wireless communication environment, an accurate channel estimation in the presence of extreme levels of frequency selectivity are not easy using the traditional PSAM techniques. Therefore another channel estimation technique MMSE has been introduced. In this scheme, the channel estimation is done by minimizing the mean square error between the estimated channel and the perfect channel by using the channel statistics and pilot symbols [36]. Recently SC-FDE has been found to be an attractive equalization technique for broadband wireless channels. We can denote the $(h(t,\theta).\mathbf{a}(\theta,\theta_i,\varphi))$ by h_{est} as is seen from the flow chart. The channel impulse response for the 60 GHz channel can be represented by the following equation as,

$$h(\tau,\theta_{rx}) = \sum_j A^j C^j \left(t-\tau^j, \theta_{rx}-\Theta_{rx}^j\right) \tag{4.4}$$

The explanation of equation 4.4 is given in chapter 2 in section channel model. The channel impulse response is analyzed for the perfect channel and also for the non-perfect channel[1] to check the performance of the algorithm after adding the Gaussian error. For most practical channel estimation schemes the error in the channel impulse response can be modeled by using the following equation.

$$\bar{h} = \hat{h}_{\theta_i} + n, \tag{4.5}$$

where $\bar{h}$ is the non-perfect channel impulse response, n is the AWGN noise and the variance of n is δ_{che}.

4.3.3 Bit Error Probability

In the fourth step bit error probability is calculated for each estimated channel impulse response $\hat{h}_{\theta_i}$. This is done for the complete range of the elevation angles. The conditional BER for the coherently detected binary modulation as derived in equation (3.10) is given by following equation.

$$\hat{P}_b\left(\mathcal{E}|\hat{h}_{\theta_i}\right) = Q\left(\sqrt{\frac{d^2}{4\delta_f^2}}\right), \tag{4.6}$$

[1] $Non-perfect$ means that we introduced a Gaussian error in the channel impulse response and for the perfect channel means there will be no error in the channel impulse response

where Q denotes the Gaussian Q function, d is $2sqrtE_b$ for BPSK (coherently detected).

$$\delta_f = \delta_N.\delta_{ch}, \tag{4.7}$$

where δ_N is the variance of the AWGN.

$$\delta_{ch} = \sum_{i=1}^{L} |g_i|^2, \tag{4.8}$$

where L represent the channel coefficients.

$$g_i = \frac{1}{N} \sum_{k=0}^{N-1} \left(\frac{1}{\hat{H}_k} \right) e^{\frac{j2\pi ki}{N}}, \tag{4.9}$$

where $\hat{H}_k = \sum_{n=0}^{N-1} \hat{h}_n e^{\frac{-j2\pi nk}{N}}$, i.e., FFT of the estimated channel and $k = 0, 1, \cdots, N-1$. This approach will work well when there is little or no error in channel estimation. For the fifth step, we impose a condition to check whether the scanning of the array steering vector is completed for the complete range of scanning angle θ_i, if the scanning is not completed then move to the first step again and do all the steps till the fourth step but if the scanning is completed then move to the sixth step.

4.3.4 DOA Estimation for Minimum BER

Now we will estimate the DOA for that response of channel for which the bit error probability $\hat{P}_{b_{\theta_i}}$ will be minimum. This can be done mathematically by the equation as,

$$\hat{h} = \min_{\hat{P}_{b_{\theta_i}}} \left[\hat{h}_{\theta_i} \right], \tag{4.10}$$

Then steer the array towards that DOA for which the $\hat{P}_{b_{\theta_i}}$ will be minimized. This is given by the following equation as,

$$\theta_i = \underset{\theta}{Arg\min} \left[\hat{P}_{b_{\theta_i}} \right], \tag{4.11}$$

Once we steer the array towards that direction for which we got the minimum bit error probability. Then by using the SC-FDE block explained in signal model of chapter 2, section 2.3, it will be straight forward to estimate the desired symbol.

The proposed beamforming algorithm contrast to the beamforming approach use in chapter 3. In chapter 3, we assume that the beam was steered towards the strongest multipath direction, whereas, in the proposed beamforming approach, the beam is steered in such a way that the interference is minimized which results in minimum BER. Therefore, in the new beamforming algorithm, the beam may not be necessarily steer towards the strongest multipath direction. Figure 4.6, shows the performance of BER with beamforming algorithm implementation in LOS and NLOS scenarios. The BER performance is computed by selecting the various values of the SNR in dB. The simulation parameters are given in the Table 4.1. It is clearly seen that the BER improves after the implementation of the proposed beamforming algorithm as compared to the one in chapter 3 without beamforming implementation. When compared to the beamforming solution of chapter 3, i.e., in which the beam is steered to the direction of the strongest multipath there is improvement also in the LOS case by using the proposed beamforming scheme as shown from the Figure 4.6.

Parameters	Values
Data length	1024
FFT length	1024
CP length	100
Number of simulation	20000
Channel environment	LOS/NLOS
Number of elements	8
Inter-element spacing	0.5λ
Sampling rate	2 GHz
Tx/Rx separation d	1 m

Table 4.1: Simulation parameters for BER with beamforming implementation.

4.4 Simulation Overview

The analysis of the proposed beamforming scheme in computing the BER will be presented for the LOS/NLOS scenarios using the arrays, i.e., an ULA and an UCA for the 60 GHz channel model. The simulation parameters are given in Table 4.2 which is used for the next subsections. The simulation is done for various physical parameters of the array geometry, i.e., M and Δ and the array scanning step size for the LOS/NLOS scenarios in perfect/non-perfect channel. The simulation will show the performance of the proposed

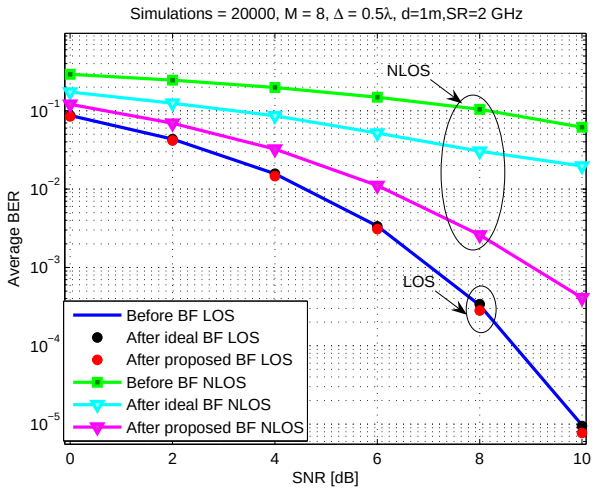

Figure 4.6: Comparison of BER with analytical and simulation with proposed beamforming algorithm.

beamforming scheme in terms of BER using the ULA and UCA antenna geometries.

Parameters	Values
Data length	1024
FFT length	1024
CP length	100
Number of simulation	20000
Channel environment	LOS/NLOS
Channel	Perfect/Non-perfect
Array scanning step	2
Sampling rate	2 GHz
Tx/Rx separation d	1 m
Signal to noise ratio (SNR)	5 dB

Table 4.2: Simulation parameters.

4.4.1 Impact of Antenna Array Elements on BER

The impact of the antenna array elements M on the BER has been investigated using the proposed beamforming scheme. The simulation results are provided by using both ULA and UCA antenna geometries in the following subsections. The simulation is performed for various number of antenna

elements and for fixed inter-element spacing Δ of the ULA and UCA.

With ULA Geometry

The impact of the antenna array elements M on BER for the ULA is plotted in the Figures 4.7 and 4.8 respectively, using the proposed beamforming algorithm for the LOS/NLOS scenarios. The perfect and non-perfect channel is considered. As seen from the Figure 4.7, the BER improves by increasing the number of the array elements M for the LOS case. From the simulation, it is seen clearly that by the implementation of the proposed beamforming algorithm, the BER improves for increasing the number of the antenna array elements M. However, the improvement is insignificant for the LOS case. It is also noted that the algorithm is error sensitive.

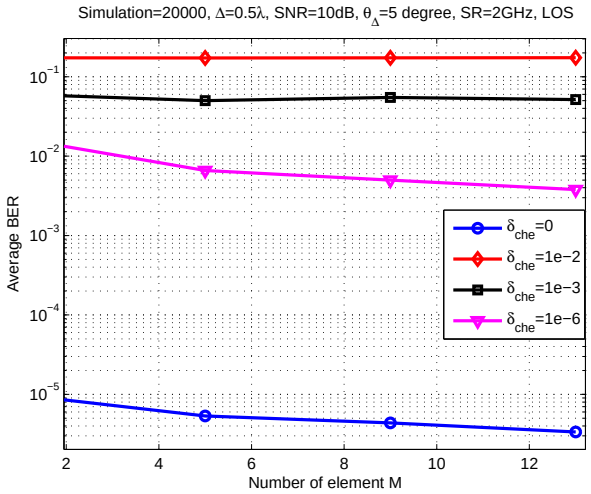

Figure 4.7: Impact of ULA M on BER in LOS case for perfect/non-perfect channel.

Figure 4.8, shows the impact of antenna array elements on BER in NLOS case. It is seen clearly from the simulation that the BER improvement is better in NLOS case by using the proposed beamforming algorithm. For both cases LOS/NLOS, the BER improves significantly upto for increasing the number of the antenna array elements M. It is mentioned in the literature [6, 9, 14, 37] that by increasing the antenna array elements M, the main lobe of the antenna array becomes narrower and the antenna array becomes more directive.

However, by increasing the elements, the side lobes will also increase but the peaks of the side lobes are smaller than the peak of the main lobe. Therefore, the antenna array locks on the strongest multipath reflection. As seen

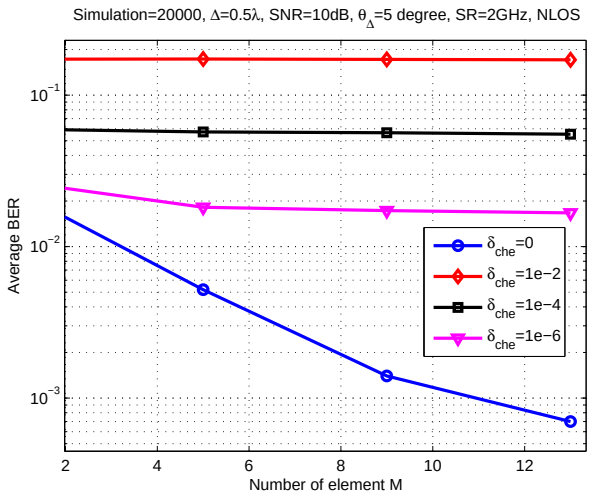

Figure 4.8: Impact of ULA M on BER in NLOS case for perfect/non-perfect channel.

from the Figures 4.7 and 4.8 for the LOS/NLOS case, the BER improvement for the LOS case is low as compared to the BER improvement for the NLOS case. It is noted from Figure 4.8, that the BER for the NLOS case also improves significantly upto the first eight antenna array elements. It is also important to note that by increasing the number of array elements, the computational complexity and the implementation cost will increase. Therefore, the antenna array elements are the trade-off between the performance and the computational complexity.

With UCA Geometry

By using the UCA, the improvement in BER can be seen in Figure 4.9 for LOS scenario. It is evident from the simulation results that the BER improves for increasing the number of array elements in LOS case after the implementation of the proposed scheme. From the simulation results, it is seen that the performance of the UCA is comparable to the ULA for LOS case. Figure 4.10 shows the impact of the UCA element M on the BER performance in NLOS case. It is noted that the BER performance is the same for the perfect channel and for the small value of channel error. The improvement of the BER for increasing the number of array elements has been seen from the simulation results because by increasing the array elements, the array becomes more directive. This means that the BER problem of broadband wireless communication is greatly reduced by using the proposed beamforming scheme with the utilization of antenna arrays.

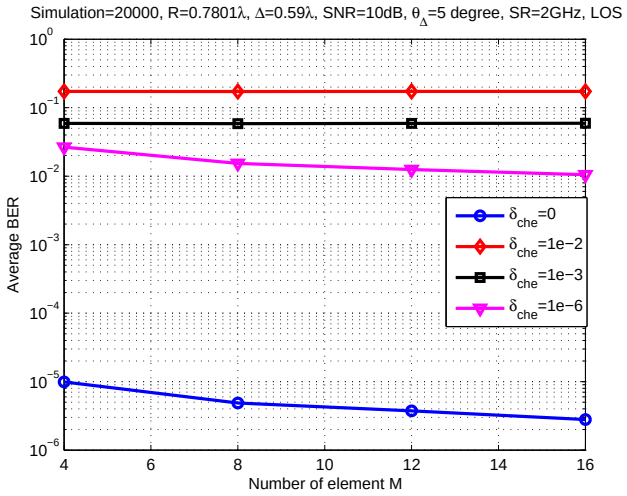

Figure 4.9: Impact of UCA M on BER in LOS case for perfect/non-perfect channel.

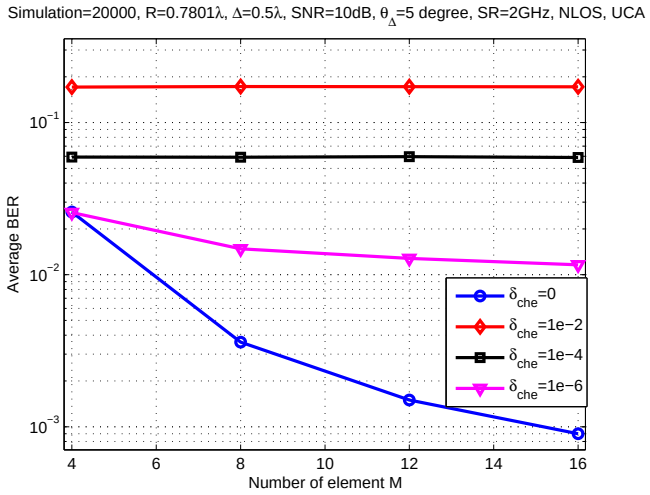

Figure 4.10: Impact of UCA M on BER in NLOS case for perfect/non-perfect channel.

It is evident from the plots that the antenna arrays show a significant improvement in BER for the first eight array elements for both cases of ULA and UCA in perfect/non-perfect channel in NLOS scenarios. By further increasing the number of array elements, the improvement in BER is insignificant. Because the increment in array elements will also increase the system computational complexity. It is therefore seen that there is a trade-off between the performance and the system computational complexity in choosing the array elements. The simulation is done for 20000 channel realizations using the 60 GHz channel, the BER is calculated for each channel realization and then averaged out for the total number of channel realizations. It seems from the above simulation that the BER for the ULA and UCA is different in LOS/NLOS cases. It is seen from the simulation plots that the algorithm is error sensitive, as is evident that for error upto $1e-2$ and $1e-4$, the BER remains same even for increasing the number of array elements.

4.4.2 Impact of Inter-element Spacing Δ on BER

The impact of the inter-element spacing Δ on the BER has been investigated using the proposed beamforming scheme. The simulation results are provided by using both ULA and UCA antenna geometries with eight array elements $M = 8$ for various values of inter-element spacing Δ in the following subsections.

With ULA Geometry

The impact of the inter-element spacing Δ of the ULA on BER is plotted in the Figures 4.11 and 4.12 respectively, using the proposed beamforming scheme for the LOS/NLOS scenarios. The values of Δ are selected as the multiples of the wavelength λ of the signal. The simulation parameters are the same as given in Table 4.2. The perfect and non-perfect channel is considered. Figure 4.11 shows that the BER improvement is not significant by increasing the inter-element spacing of the ULA array for the LOS scenario in perfect channel. However, the improvement is significant in case of non-perfect channel.

It is noted from the Figure 4.11 that if near ideal channel estimates are available one can actually make smaller arrays (less than 0.5λ). It is seen from the plot that the BER improves upto a certain value of the Δ. After that value of Δ, the improvement in the BER starts decreasing because for the increment in Δ the strength of the side lobe increases which results in decreasing the improvement of the BER. Figure 4.12 shows the impact of

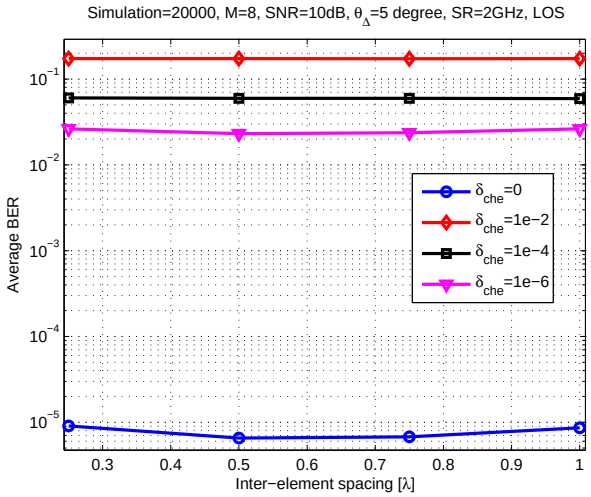

Figure 4.11: Impact of Δ on BER in LOS case for perfect/non-perfect channel.

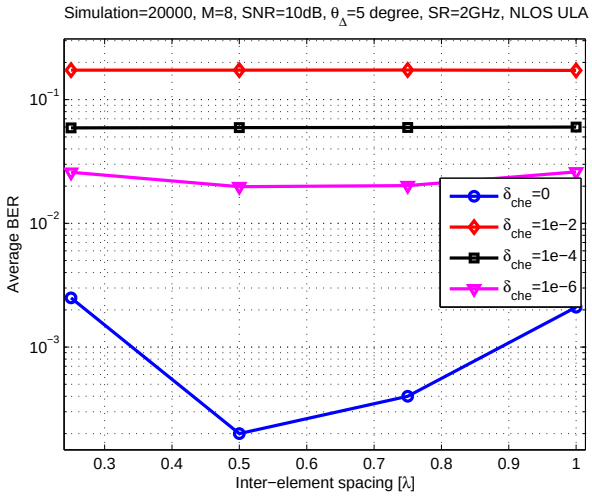

Figure 4.12: Impact of Δ on BER in NLOS case for perfect/non-perfect channel.

the Δ on the BER performance. It is noted that Δ has significant effect in perfect channel and also for the non-perfect channel for small error.

With UCA Geometry

Figure 4.13, shows the impact of the inter-element spacing Δ of the UCA in LOS case. There is a relationship between the inter-element spacing Δ and R of the UCA as given in equation (3.1) which shows that if the radius R is large, then the Δ will also be large for the same number of array elements. From the plots, it is noted that the performance for the ULA and the UCA is comparable for the LOS case. For the NLOS case, the impact of the inter-element spacing Δ on the BER can be seen from the Figure 4.14 in perfect and non-perfect channel for the small error. The BER performance improves for an optimum value of the Δ , i.e., 0.5λ of the ULA and the optimum value of Δ, i.e., 0.59λ of the UCA which is different from the previous value of Δ of UCA investigated in chapter 3. During simulations, the perfect/non-perfect channel for the LOS/NLOS scenarios are considered.

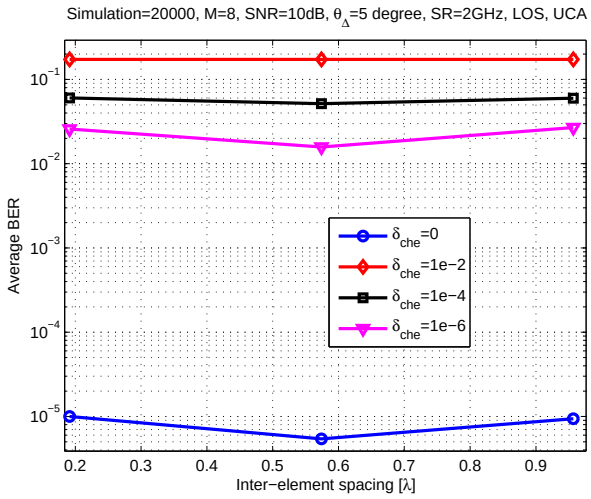

Figure 4.13: Impact of UCA R on BER in LOS case for perfect/non-perfect channel.

It is noted from the Figure 4.13 that if near ideal channel estimates are available one can actually make smaller arrays (less than 0.5λ). By implementation of the proposed beamforming scheme, it is proved that the BER improves upto the half wavelength value of the Δ which is mentioned in literature [9, 19, 38]. Also we investigate the optimum value of the radius R and Δ of the UCA which gives better performance for the beamforming of 60 GHz transceiver system.

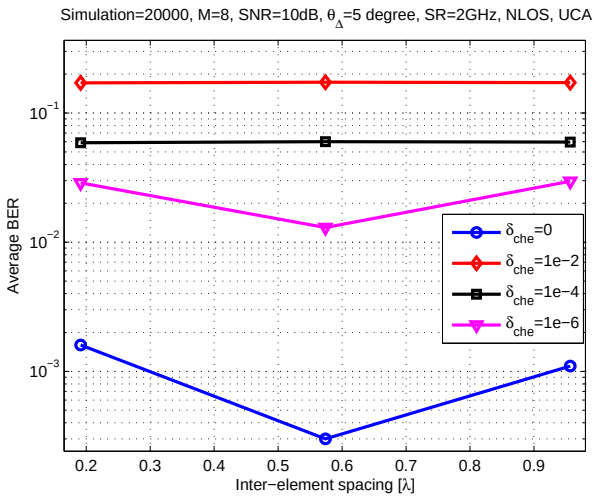

Figure 4.14: Impact of UCA R on BER in NLOS case for perfect/non-perfect channel.

4.5 Beamforming Gains at 60 GHz

The BER has been computed by using the proposed beamforming algorithm for the 60 GHz channel model. The BER performance is computed by selecting physical parameters investigated from the simulation results above for various values of the SNR in dB. For $M = 8$, the optimum value of the inter-elements spacing Δ of the ULA and the UCA is taken. The simulation parameters for the ULA and UCA are given in Table 4.3. For ideal CSI, BER can be computed using equation (3.10), while for imperfect CSI, Monte Carlo simulations are used. For each channel realization, we compute the BER and then average over all the channel realizations. The results are plotted against the SNR for the ULA and the UCA. The simulation was performed for the 60 GHz channel model and the effects of utilizing the physical parameter with ideal beamforming implementation, on the BER were investigated.

It is seen from the Figures 4.15, 4.16, 4.17 and 4.18 respectively that the BER improves for both the LOS/NLOS scenarios by implementing the proposed beamforming scheme. The improvement is seen in both cases for perfect and non-perfect channel. The simulation parameters are given in Table 4.3. It is seen from the plots 4.15 and 4.17 respectively that the BER performance is for both the array geometries (ULA and UCA) are comparable for LOS/NLOS scenarios. It is therefore, concluded that the proposed beamforming scheme shows better performance in perfect channel and non-perfect channel for small error.

Parameters	Values
Data length	1024
FFT length	1024
CP length	100
Number of simulation	20000
Channel environment	LOS/NLOS
Channel	Perfect/Non-perfect
Array elements M	8
Inter-element spacing Δ	0.5λ
Radius R	0.7801λ
Inter-element spacing of UCA	0.59λ
Array scanning step	5
Sampling rate	2 GHz
Tx/Rx separation d	1 m

Table 4.3: Simulation parameters for beamforming gain at 60 GHz.

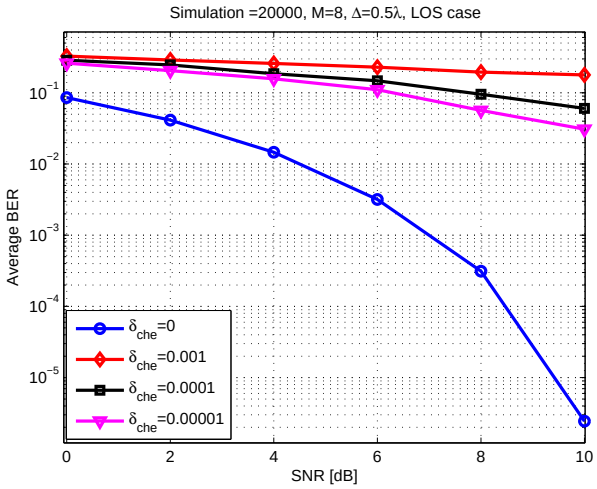

Figure 4.15: Beamforming gains in LOS case with ULA.

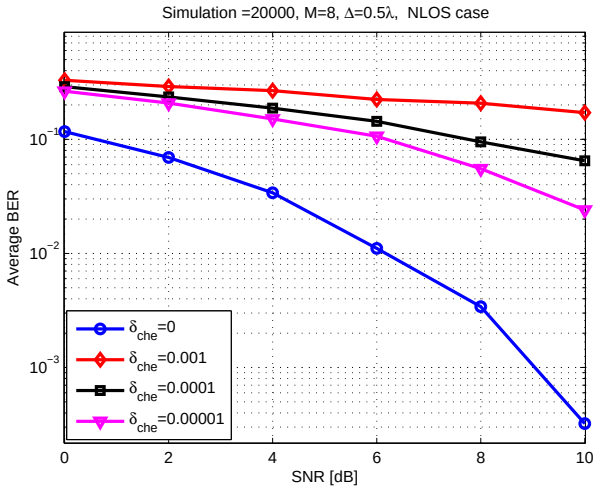

Figure 4.16: Beamforming gains in NLOS case with ULA.

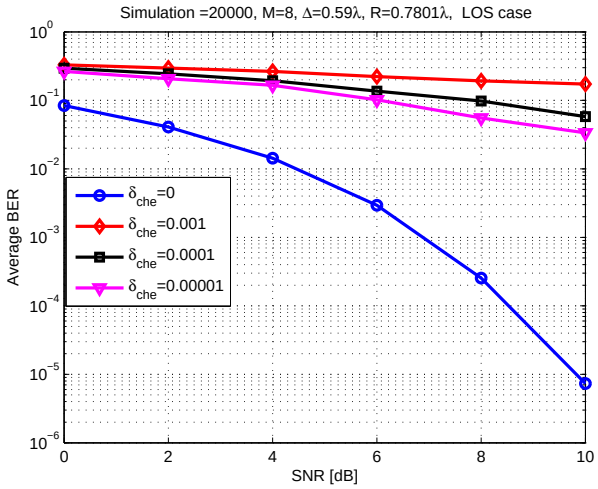

Figure 4.17: Beamforming gains in LOS case with UCA.

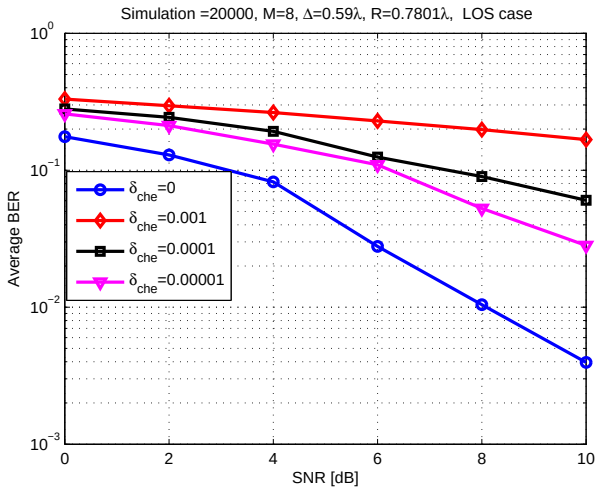

Figure 4.18: Beamforming gains in NLOS case with UCA.

4.6 Impact of Array Scanning Step Size on BER

The array scanning step size θ_Δ is an important parameter to be considered for the proposed beamforming algorithm. The simulations for the various scanning step size θ_Δ have been done using the proposed beamforming scheme for the 60 GHz channel model. The simulation parameters are the same as given in Table 4.3 except for the various values of scanning step size θ_Δ rather than the SNR. The BER performance has been computed for various number of array elements M for each scanning step size. Figure 4.19 shows the impact of the scanning step size θ_Δ on the BER utilizing the antenna array with the proposed beamforming scheme in NLOS scenarios. The variation in the average BER has been investigated by changing the scanning step of the array steering vector. The channel coding is not considered in the proposed beamforming scheme. It is seen from the Figure 4.19, that the θ_Δ has significant effect of scanning step size with increasing the number of antenna array elements. It is evident that the difference in BER is significant by selecting the scanning step size θ_Δ equal to 1° or 20°. It is seen from the simulation results that scanning step size with value 1° shows lower BER as compared to the BER value at 20° with same number of array elements.

Figure 4.19 shows that a BER of 10^{-3} can be achieved with 1 degree step size and 5 elements or 5 degree step size with 6 elements or the 10 degree step size with 7 elements or the 15 degree step size with 9 elements or the 20 degree step size with 11 elements. It means that there is trade-off between the

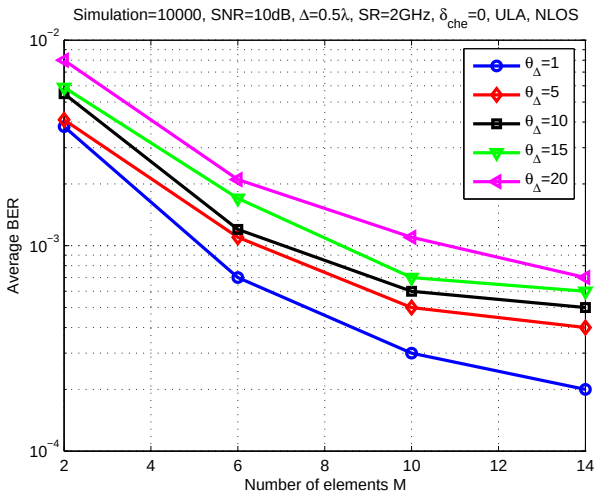

Figure 4.19: Impact of scanning step size on BER in NLOS case $\Delta = 0.5\lambda$, $SNR = 10dB$.

scanning step size θ_Δ and number of array elements M. It is therefore a better option in choosing the scanning step size θ_Δ between 1° and/or 20° with the choice of number of array elements as can be seen from the simulation result. It is also considerable that for the greater value of the scanning step size θ_Δ the processing will be fast and the computational complexity will be decreased with the expense of BER performance. Therefore, there is also a trade-off between the computational complexity and the average BER performance in selecting the step size for the beamforming of 60 GHz transceiver system.

4.7 Conclusion

In this chapter a new beamforming algorithm was proposed for the 60 GHz transceiver system. It was seen that the physical parameters, i.e., the number of antenna array element M and the inter-element spacing Δ the ULA and the UCA gives significant improvement in BER with the implementation of the proposed beamforming algorithm. It is therefore concluded from the presented simulation results that the BER improves by using the new beamforming algorithm. The simulation is performed in the LOS/NLOS scenarios and in both cases it was seen that the BER improves for the optimum value of the inter-element spacing Δ, i.e.,0.5λ of the ULA and , i.e.,0.59λ of the UCA respectively with an eight number of array elements. It is also noted that the proposed beamforming algorithm is error sensitive, since for large error, it has no effect on the BER performance. From the simulation results, it was seen that there is a trade-off between the array scanning step size and the number of array elements. It is also investigated that the computational complexity of the beamforming algorithm is rather less intensive by choosing the large scanning step size θ_{Δ}.

Chapter 5

Final Conclusions

In this thesis, a beamforming scheme has been investigated for the 60 GHz transceiver system. The conclusion of the thesis is organized as follows,

- **Chapter 1**, a brief introduction of the 60 GHz was explained and then the crucial problem of the 60 GHz was identified. Different challenges and advantages of the 60 GHz were presented.
- **Chapter 2**, presents two basic antenna array structures, i.e., linear and circular. In this chapter a simplified mathematical SC-FDE based signal model was presented. Then the channel model was presented along with the different important parameters such as power delay profile, time delay spread and coherence bandwidth.
- **Chapter 3**, presents the antenna array considerations. An ideal beamforming scheme has been considered in which the DOA of all the multipath are known and the array has been steered to the strongest multipath. It provides simulation results which shows the impact of the physical parameters of the antenna array on the RMS delay spread and the average BER. It was seen that by increasing the number of array elements, the RMS delay spread and the BER improves significantly in LOS/NLOS scenarios. However, the RMS delay spread and the BER also improve for an optimum value of the inter-element spacing of the ULA and the radius of the UCA. However, the optimum values for the Δ and R has been observed which is 0.5λ and 0.8701λ respectively, in both LOS/NLOS scenarios.
- **Chapter 4**, a new low complexity (hardware wise) beamforming scheme for the 60 GHz transceiver systems was proposed. Then the performance of the scheme has been observed by changing the various antenna array physical parameters. ULA and UCA are compared for

the proposed beamforming algorithm, the effects of the ULA and UCA physical parameters in LOS/NLOS case by introducing the δ_{che} are investigated. It has been seen that the physical antenna array parameters have great impact on the RMS delay spread and the BER performance with the implementation of new beamforming algorithm. The optimum values $\Delta = 0.5\lambda$ of ULA and $R = 0.7801\lambda$ and $\Delta = 0.59\lambda$ of UCA has been obtained in LOS/NLOS case. By choosing those optimum values of Δ and R obtained from the simulations, the problems of 60 GHz, i.e., BER and RMS delay spread are greatly reduced. Since by increasing the number of antenna array elements M, the implementation complexity of the system increase. Therefore, a suitable number of antenna array elements have been defined which give acceptable performance with the new beamforming algorithm. It is also investigated that there is trade-off between the scanning step size θ_{Δ} and number of array elements M. It is therefore concluded that the proposed beamforming algorithm is less complex hardware wise and also low cost. Since SC-FDE scheme has been considered, it is also a power efficient scheme because of low IBO power requirement of power amplifier.

5.1 Future Work

The proposed scheme for the RF level beamforming is complex due to the small scanning step size of the array steering vector although it is simple hardware wise and low cost. Therefore, the following future work can be possible.

- low complexity blind estimation schemes should be investigated.
- the proposed algorithm is error sensitive which should be investigated and improve this sensitivity.
- we can implement the classical beamforming algorithm for more accuracy but the complexity will be increased. The implementation of the classical beamforming algorithm will be possible, if we do the beamforming element wise. For one element take the amplitude one and put all others equal to zero and do the scanning for this element, then perform this procedure for the whole array element by which the scheme will be more computationally complex.
- we have not considered the channel coding with the proposed algorithm. Therefore, the extension of this algorithm with the channel coding can also be the future work.

Bibliography

[1] P. Smulders, *60 GHz radio at home.* Eindhoven University of Technology.

[2] *Performance characteristics on 60 GHz communication system.* Terabeam Corporation, Oct 2002.

[3] L. Caetano and S. Li, *Benefits of 60 GHz: Right frequency, Right time.* SiBEAM, wireless beyond boundries, Nov 2005.

[4] A. Goldsmith, *Wireless Communications.* Cambridge University press, 2005.

[5] H. Yang, P. Smulders, and H. Herben, "Frequency selectivity of 60-ghz los and nlos indoor radio channels," vol. 6. Vehicular Technology Conference VTC, May 2006, pp. 2727–2731.

[6] P. Stoica and R. Moses, *Introduction to Spectral Analysis.* New York, NY: Prentice Hall, 1997.

[7] L. C. Godara, "Applications of antenna arrays to mobile communications, partii: Beam-forming and direction-of-arival considerations," in *Proc. IEEE*, vol. 85, August 1997, pp. 1195–1245.

[8] F. Gross, *Smart Antennas for Wireless Communications.* NY, USA: McGraw-Hill, 2005.

[9] A. Veen and G. Leus, *Signal Processing for Communications*, et-4147 ed. NY, USA: TU Delft, 2005.

[10] L. C. Godara, "Applications of antenna arrays to mobile communications, parti: Performance improvement, feasibility, and system considerations," in *Proc. IEEE*, vol. 85, July 1997, pp. 1031–1060.

[11] R. H. Roy, *ESPRIT, Estimation of Signal Parameters via Rotational Invariance Techniques.* Stanford, CA: Stanford University, August 1987.

[12] D. Falconer, S. L. Ariyavisitakul, A. Benyamin-Seeyar, and B. Eidson, "Frequency domain equalization for single-carrier broadband wireless systems," vol. 40. IEEE Communications Magazine, April 2002, pp. 58–66.

[13] P. Baltus, P. F. M. Smulders, and Y. Yu, "Systems and architectures for very high frequency radio links," *Analog Circuit Design*, pp. 2179–2190, October 2001.

[14] P. S. Naidu, *Modern Digital Signal Processing, an Introduction*. Oxford, U.K: Alpha Science, 2006.

[15] R. Monzingo and T. Miller, *Introduction to Adaptive Arrays*. New York, NY: John Wiley & Sons, 1980.

[16] S. Haykin, *Adaptive Filter Theory*. New York, NY: Prentice Hall, 1986.

[17] L. Rakotondrainibe, G. Zaharia, G. El Zein, and Y. Lostanlen, *Indoor Channel Measurements and Communications System Design at 60 GHz*. [online]: ursi-test.intec.ugent.be/files/URSIGA08/papers/C10p3.pdf, 2008.

[18] U. H. Rizvi, "Comparison of suitable modulation and coding schemes based on a first evaluation," *SiGi Spot Project Deliverable D5.2*, pp. 1–42, April 2007.

[19] J. Litva and T. K. Lo, *Digital Beamforming in Wireless Communication*. Norwood: Artech House, 1996.

[20] A. Maltsev et al, "Channel models for 60 ghz wlan systems." IEEE 802.11, Wireless LANs, Intel, March 2009.

[21] H. Yang, P. F. M. Smulders, and M. H. A. J. Herben, "Channel characteristics and transmission performance for various channel configurations at 60 GHz," *EURASIP Journal on wireless communication*, 2007.

[22] C. Balanis, *Antenna Theory*. New Jersey: Wiley, 2005.

[23] S. Yong and C. Chong, "An overview of multigigabit wireless through millimeter wave technology: Potentials and technical challenges." Hindawi Publishing Corporation, EURASIP Journal on Wireless Communications and Networking, 2007.

[24] H. Nam, *Statistical Analysis of Indoor Radio Propagation Channel Characteristics at 60GHz*. Austin, USA: The University of Texas at Austin, Wireless Networking and Communications Group.

[25] V. Erceg, *VHT 60 GHz Channel Model Recommendation*. Broadcom corporation, May 2008.

[26] T. Rappaport, *Wireless Communications: Priciples and Practice*, 2nd ed. Prentice Hall, New York, 2002.

[27] U. H. Rizvi, "Low cost acoustic demonstrator for 60 ghz baseband implementation," *SiGi Spot Project Deliverable D5.3*, pp. 1–40, October 2008.

[28] S. Kingsley and S. Quegan, *Understanding Radar Systems*. USA: Sci TechPublishing, Inc, 1999.

[29] W. H. Tranter, K. S. Shanmugan, T. S. Rappaport, and K. L. Kosbar , *Principles of Communication Systems Simulation with Wireless Applications*. NJ, USA: Prentice Hall, 2004.

[30] M. Brandstein and H. Silverman, *A practical methodology for speech localization with microphone arrays*. Brown University: Technical Report, Brown University, November 1996.

[31] R. Roy and T. Kailath, "Esprit - estimation of signal parameters via rotational invariance techniques," in *IEEE Transaction on Acoustics, Speech Signal Processing*, July 1989, pp. 984–995.

[32] B. Ottersten, M. Viberg, and T. Kailath, "Performance analysis of the total least squares esprit algorithm," in *IEEE Transaction on Signal Processing*, May 1991, pp. 1122–1135.

[33] J. K. Cavers, "An analysis of pilot symbol assisted modulation for rayleigh fading channels," in *IEEE Transaction on Vehicular Technology*, 2005.

[34] M. Medard, I. Abou-Faycal, and U. Madhow, "Adaptive coding for pilot symbol assisted modulation without feedback," in *IEEE Transaction on Communication Magazine*, vol. 40, no. 4, Nov. 2005, pp. 686–693.

[35] J. A. C. Bingham, "Multicarrier modulation for data transmission: An idea whose time has come," in *IEEE Communications Magazine*, vol. 28, May 1990, pp. 5–14.

[36] F. W. Vook and T. Thomas, "Mmse multi-user channel estimation for broadband wireless communications," in *in Proc. IEEE Global Telecommunications Conference (GLOBECOM 01)*, vol. 1, Nov. 2001, pp. 470–474.

[37] N. K. Bose and C. R. Rao, *Signal processing and its application: Handbook of Statistics 10*. North-Holland: North-Holland, 1993.

[38] C. R. Johnson and W. A. Sethares, *Telecommunication Breakdown; concept of communication transmitted via software-defined radio*. Prentice Hall, February 2003.